Cooperative Impedance Control for Multiple Underwater Vehicle Manipulator Systems under Lean Communication

Shahab Heshmati-Alamdari, Charalampos P. Bechlioulis, George C. Karras and Kostas J. Kyriakopoulos

***Abstract*—This paper addresses the problem of cooperative object transportation for multiple Underwater Vehicle Manipulator Systems (UVMSs) in a constrained workspace with static obstacles, where the coordination relies solely on implicit communication arising from the physical interaction of the robots with the commonly grasped object. We propose a novel distributed leader-follower architecture, where the leading UVMS, which has knowledge of the object's desired trajectory, tries to achieve the desired tracking behavior via an impedance control law, navigating in this way, the overall formation towards the goal configuration while avoiding collisions with the obstacles. On the other hand, the following UVMSs estimate locally the object's desired trajectory via a novel prescribed performance estimation law and implement a similar impedance control law that achieves tracking of the desired trajectory despite the uncertainty and external disturbance in the object and the UVMS dynamics respectively. The feedback relies on each UVMS's force/torque measurements and no explicit data is exchanged online among the robots, thus reducing the required communication bandwidth and increasing robustness. Moreover, the control scheme adopts load sharing among the UVMSs according to their specific payload capabilities. Finally, various simulation studies clarify the proposed method and verify its efficiency.**

***Index Terms*—Underwater Vehicle Manipulator System, Underwater Cooperative Manipulation, Marine Robotics, Implicit communication, Cooperative manipulation.**

I. Introduction

During the last decades, significant progress has been made in the field of Unmanned Underwater Vehicles (UUVs), making them an imperative enabler for a variety of maritime activities [1] such as ocean forecasting [2], marine science (e.g., deep see exploration [3], ecosystem monitoring [4], archaeology [5]) and offshore industry applications (e.g., ship maintenance, inspection of oil/gas facilities) [6], [7]. However, there is a vast number of applications that go beyond the survey activities and demand the underwater vehicle to be enhanced with intervention capabilities as well [8], thus raising increasing interest on Underwater Vehicle Manipulator Systems (UVMSs) [9]. Nowadays, the underwater intervention tasks involve a Remotely Operated Vehicle (ROV), equipped with one or multiple manipulators that allow it to grasp, transport and manipulate objects while being controlled by a human pilot on a surface ship, via a master-slave tele-operation scheme [10]–[13]. However, to meet this growing demand and due to the well-known disadvantages of human-robot tele-operation (e.g., time delays, increase of human fatigue over time), the development of autonomous intervention control schemes for UVMSs have gained significant scientific attention during the last thirty years [14]–[16].

More specifically, during late 90s, early efforts towards designing and developing grippers for underwater manipulation were made within the pioneering project AMADEUS [17] where the problem of dual arm manipulation was studied and validated experimentally in a water tank [18]. The aforementioned results were exploited later in both the UNION project [19] as well as the SAUVIM project [14], where for the first time autonomous underwater free-floating intervention was carried out. In the last decade, research on autonomous underwater interaction tasks has been enhanced by a various number of projects. Among them, a significant boost was given by the European project TRIDENT [20]–[25], where a complex vehicle-arm system consisting of a vehicle of comparable mass with its manipulator, was controlled in a coordinated manner to demonstrate underwater free-floating intervention. A turning point in vehicle-arm coordination was given in the MARIS project [26] where various performance metrics on the vehicle-arm system were taken into account. Another important milestone was achieved within the PANDORA project [27]–[29], where a strong emphasis was given on the problem of persistent autonomy. One of the most recent project in the domain of underwater intervention was the EU H2020 DexRov [30]–[33] which focused on inspection and maintenance tasks via satellite communications in the presence of latencies. Finally, the most recent research effort towards this direction is the on-going European project SeaClear [34], which by employing autonomous underwater robots aims to develop a collaborative, heterogeneous multi-robot solution engaged in collecting marine waste.

It should be noted that most of the underwater manipulation tasks can be carried out more efficiently, if multiple UVMSs are cooperatively involved. For instance, two or more UVMSs can transport bulky objects (see Fig. 1) more easily and safely than a single UVMS, owing to shape, actuation and payload constraints [35], [36]. In [35], the authors have studied the problem of modeling two UVMSs carrying a rigid object. The robot-object contact was considered rigid, thus the whole system configuration formed a singular system of differential equations [37]. The kinematic redundancy and manipulability of this system were examined in [38], [39]. Moreover, a centralized cooperative control scheme for multiple UVMSs holding commonly an object was proposed in [36]. However,

Shahab Heshmati-alamdari is with the Division of Decision and Control Systems, School of Electrical Engineering and Computer Science, KTH Royal Institute of Technology, Stockholm SE-10044, Sweden, Email: shaha@kth.se. G. C. Karras, is with the University of Thessaly, Dept. of Computer Science and Telecommunications, 3rd Km Old National Road Lamia - Athens, 35100, Lamia, Greece, and the Control Systems Laboratory, School of Mechanical Engineering, National Technical University of Athens, Athens 15780, Greece, Emails: gkarras@uth.gr, karrasg@mail.ntua.gr. C. P. Bechlioulis and K. J. Kyriakopoulos are with the Control Systems Lab, School of Mechanical Engineering, National Technical University of Athens, Greece. Emails:{chmpechl,kkyria@mail.ntua.gr}. (Corresponding author: Shahab Heshmati-alamdari).

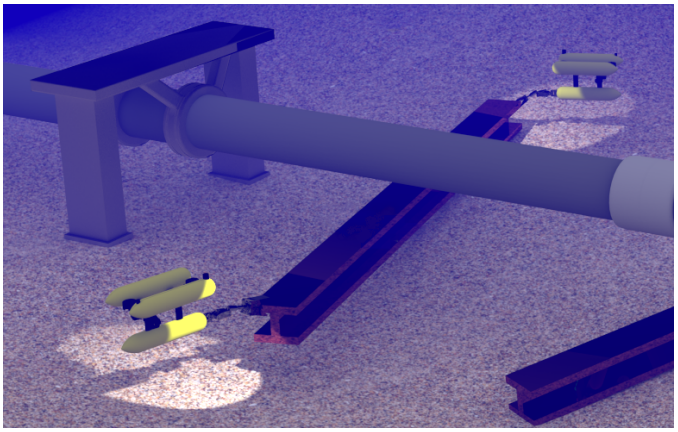

Fig. 1. A cooperative transportation task conducted by UVMSs.

in all aforementioned works, the major requirements and constraints imposed by the nature of underwater environment have not been considered at all.

Underwater tasks are very demanding, with the most significant challenge being imposed by the strict communication constraints [14], [40]. In general, the communication of multi-robot systems can be classified in two major categories, namely explicit and implicit. The first one is designed solely to convey information such as control signals or sensory data directly to other robots [41], while the latter occurs as a side-effect of robots' interaction with the environment or other robots, either physically (e.g., the interaction forces between the object and the robot) or non-physically (e.g., visual observation). Nevertheless, in the latter case, the required information is acquired by appropriate sensors installed on the robots (e.g., force/torque or vision sensors). Hence, the most investigated and frequently employed communication form in multi-robot systems is the explicit one. It usually leads to simpler theoretic analysis and renders teams more effective. However, even though the inter-robot communication is of utmost importance during cooperative manipulation tasks, employing explicit communication in underwater environment may result in severe performance issues owing to the limited bandwidth and update rate of underwater acoustic devices. Moreover, as the number of cooperating robots increases, communication protocols require complex design to deal with the crowed bandwidth [42]. Therefore, the number of operating underwater robots, involved in cooperative schemes that exploit explicit communication protocols, is strictly limited owing to the narrow bandwidth of acoustic communication devices. In order to overcome such limitations, implicit communication can be employed instead. Despite the increased difficulty of the theoretical analysis, it leads to simpler protocols and saves bandwidth as well as power, since no or very few data is explicitly exchanged.

Cooperative manipulation has been well-studied in the literature, especially the centralized schemes [43]–[47]. Despite its efficiency, centralized control is less robust, since all units rely on a central system, and its complexity increases rapidly as the number of participating robots becomes large. On the other hand, although decentralized cooperative manipulation schemes exhibit increased robustness and low complexity, they usually depend on either explicit communication among the robots (e.g., online transmission of the desired trajectory [48], [49] or off–line knowledge of the objects' trajectory [50]–[52]). For instance, in order to achieve collision avoidance, either the desired object trajectory should be transmitted online between the cooperating underwater robots or all robots should agree mutually on a safe desired trajectory of the object in the workspace. This demands an accurate common global localization system for all participating robots [53], which either is difficult to be achieved in underwater environment or in the most optimistic case would raise the mission cost. Therefore, the design of decentralized cooperative manipulation algorithms for underwater tasks employing implicit and lean explicit communication becomes apparent. In recent studies [53], [54], potential fields methods were employed and a multi-layer control structure was developed to manage the coordination of the robot swarm, the guidance and navigation of UVMSs and the manipulation tasks. To overcome localization and consensus problems, the authors have considered the object as the swarm reference frame. However, employing this strategy, requires each robot to communicate with the whole robot team, which consequently restricts the number of robots involved in the cooperative manipulation task owing to bandwidth limitations. Compelling results towards the same direction have been presented in [55]–[57], based on the priority control strategy [58]. In particular, a three-fold decentralized cooperative control strategy is proposed, where initially each robot finds out an individual optimal task space control velocity, which is transfered afterwards among the robots in order to obtain a commonly agreed velocity via a fusion policy. The commonly agreed task velocity then is extended to the joint space of each UVMS based again on a task priority technique [58], but this time with a higher priority. Various safety constraints (e.g., joint limits, manipulability) may also be considered in case of two cooperating UVMSs. However, the implementation of the aforementioned scheme for a large number of cooperative UVMSs, should also deal with crowed bandwidth issues. Moreover, if constrained workspace (i.e., obstacles within the workplace) is considered, achieving consensus on a mutually agreed safe trajectory would become questionable.

In this work[1], the problem of cooperative object transportation considering multiple UVMSs in a constrained workspace with static obstacles is addressed. The challenge lays in replacing explicit communication with implicit, by incorporating feedback that results from the physical interaction of the robots with the commonly grasped object (i.e., we assume that each UVMS is equipped with a force/torque sensor attached on its end-effector). The proposed scheme is based on a leader-follower architecture, where the leader, which is aware of the object's desired trajectory, tracks it via an impedance control law. On the other hand, the followers estimate the desired

[1]A preliminary version of this work has been accepted to IEEE OES Autonomous Underwater Vehicle Symposium, 2018" [59]. In the current version, a more detailed analysis of the methodology, including stability analysis, along with an enriched set of numerical simulation results with more challenging cases and a comparative simulation study regarding to centralized case using explicit communication among the UVMS team are provided in addition.

trajectory in a distributed way, via observing the object motion, and impose a similar impedance law. All impedance laws linearize the dynamics and incorporate coefficients for load sharing. The estimation process is based on the prescribed performance methodology [60] that drives the estimation error to an arbitrarily small residual set. Moreover, appropriate adaptive laws have been designed to compensate for the parametric uncertainty of the UVMSs dynamics as well as the external disturbances. Finally, it should be noticed that the proposed scheme exploits information, i.e., force/torque at the end-effector, position and velocity measurements, acquired solely by onboard sensors (e.g., via a fusion algorithm on measurements of various sensors such as F/T sensor, IMU, USBL and DVL), avoiding thus any tedious inter-robot explicit communication.

One should bear in mind that although underwater vehicles are equipped with acoustic modems to communicate with the surface control station[2], employing implicit communication based cooperative control protocols is clearly motivated by the limited bandwidth of acoustic communication devices. Moreover, in order to achieve collision avoidance, either the leader has to transmit online the desired object trajectory to the followers, or all UVMSs should obtain a mutually agreed desired trajectory of the object, which necessitates for an accurate common localization system [53] that is extremely challenging and prone to errors in underwater environments. On the contrary, in the proposed scheme, it is worth noting that each follower estimates locally and in a distributed way the desired object trajectory relatively to its inertial frame, employing exclusively its own measurements (position, velocity and force/toque). In this way, although the proposed control strategy does not remove all practical needs for communication in underwater intervention tasks, (e.g., for safety, adaptability and efficiency) nevertheless, it relieves the team from intense inter-robot communication during the execution of the collaborative tasks. This, consequently, increases significantly the robustness of the cooperative scheme and furthermore avoids any restrictions imposed by the acoustic communication bandwidth (e.g., the number of participating UVMSs). Additionally, the estimation algorithm employed in this work (for object's desired trajectory estimation) is more robust with respect to the algorithms employed in corresponding works on implicit communication-based cooperative manipulation presented in [61], [62], since it can converges even though the desired object's acceleration profile is non-zero (i.e., for an arbitrary object's desired trajectory profile as long as it is bounded and smooth). Finally, the customizable ultimate bounds allow us to achieve practical stabilization of the estimation error, with accuracy limited only by the sensors' resolution.

The rest of the manuscript is organized as follows: Section II introduces the problem and describes the system model. The proposed control methodology is presented in Section III. Section IV validates our approach via simulated paradigms. Finally, Section V concludes our work.

[2]For example, all cooperating UVMSs need to know the initial position of the object to be transported, in order to reach and grasp it, and coordinate discrete phases of the tasks via simple high level messages (e.g., "Ok, I've grasped it", "Let us proceed").

II. Problem Formulation

Consider $N+1$ UVMSs under a single leader - multiple followers architecture, rigidly grasping an object[3] in a constrained workspace with static obstacles (see Fig 1). We also assume that each vehicle is actuated in all 6 Degrees of Freedom (DoFs) and is equipped with an n DoFs manipulator. Thus, each UVMS is fully-actuated at its end-effector frame. This assumption implies that all UVMSs are able to exert arbitrary forces and torques on the object along and around any direction. It should also be noted that in the proposed scheme, only the leading robot is aware of the obstacles' position in the workspace and the object's desired configuration $\boldsymbol{x}_o^d$. On the other hand, the followers estimate locally in a distributed way the object's desired trajectory profile and manipulate the object in coordination with the leader based solely on their own sensory information. Moreover, we assume that the UVMSs are equipped with appropriate sensors, that allow them to measure their position and velocity (e.g., employing a fusion technique based on measurements by various onboard sensors such as USBL, IMU, DVL and depth-sensor), as well as the interaction forces/torques with the object via a force/toque sensor. Additionally, the geometric parameters of both the UVMSs and the commonly grasped object are considered known, whereas their dynamic parameters are completely unknown. Moreover, the control of each UVMS will be designed based on a commonly agreed frame on a specific feature of the object, which could be identified employing a visual detection system, owing to the fact that the limited underwater visibility is not an issue when all robots are close to the object of interest. Notice that owing to: i) the strict communication constraints (i.e., online inter-robot communication is not permitted), ii) the model uncertainties of UVMSs (common problem in underwater robotics) and iii) the constrained workspace, the problem becomes very challenging, with no previously reported results in the related literature.

A. Kinematics

Consider $N+1$ UVMSs operating in a bounded workspace $\mathcal{W} \subseteq \mathbb{R}^3$. We denote the coordinates of the commonly agreed body-fixed frame on the object as well as the leader's and followers' task space (i.e., end-effector) coordinates by $\boldsymbol{x}_O = [\boldsymbol{\eta}_{1,O}^\top, \boldsymbol{\eta}_{2,O}^\top]^\top$, $\boldsymbol{x}_L = [\boldsymbol{\eta}_{1,L}^\top, \boldsymbol{\eta}_{2,L}^\top]^\top$ and $\boldsymbol{x}_{F_i} = [\boldsymbol{\eta}_{1,F_i}^\top, \boldsymbol{\eta}_{2,F_i}^\top]^\top$, $i \in \mathcal{N} = \{1, \ldots, N\}$ respectively. More specifically, $\boldsymbol{\eta}_{1,i} = [x_i, y_i, z_i]^\top$ and $\boldsymbol{\eta}_{2,i} = [\phi_i, \theta_i, \psi_i]^\top$, $i \in \{O, L, F_1, \ldots, F_N\}$ denote the position and the orientation expressed in Euler angles representation with respect to the inertial frame. Alternatively, the orientation coordinates $\boldsymbol{\eta}_{2,i}$, $i \in \{O, L, F_1, \ldots, F_N\}$ expressed in the Euler angles may be described by a rotation matrix $\boldsymbol{R}_i = [\boldsymbol{n}_i, \boldsymbol{o}_i, \boldsymbol{\alpha}_i] \in \mathbb{R}^3$, $i \in \{O, L, F_1, \ldots, F_N\}$, where $\boldsymbol{n}_i$, $\boldsymbol{o}_i$ and $\boldsymbol{\alpha}_i$ are its corresponding columns [63]. Let $\boldsymbol{q}_i = [\boldsymbol{q}_{v,i}^\top, \boldsymbol{q}_{m,i}^\top]^\top \in \mathbb{R}^{6+n}, i \in \mathcal{K} = \{L, F_1, \ldots, F_N\}$ be the joint state variables of each UVMS, where $\boldsymbol{q}_{v,i} \in \mathbb{R}^6$ is the vector that involves the

[3]The end-effector frame of each UVMS is always constant relative to the object's body fixed frame.

position and orientation of the vehicle and $\boldsymbol{q}_{m,i} \in \mathbb{R}^n$ is the vector of the angular positions of the manipulator's joints. Let also define the object as well as the leader's and followers' end effector generalized velocities by $\boldsymbol{v}_O = [\dot{\boldsymbol{\eta}}_{1,O}^\top, \boldsymbol{\omega}_O^\top]^\top$, $\boldsymbol{v}_L = [\dot{\boldsymbol{\eta}}_{1,L}^\top, \boldsymbol{\omega}_L^\top]^\top$ and $\boldsymbol{v}_i = [\dot{\boldsymbol{\eta}}_{1,i}^\top, \boldsymbol{\omega}_i^\top]^\top,\ i \in \{F_1, \ldots, F_N\}$, where $\dot{\boldsymbol{\eta}}_{1,i}$ and $\boldsymbol{\omega}_i$ denote the linear and angular velocity with respect to the inertial frame respectively. Without any loss of generality, for the augmented UVMS system we get [15]:

$$\boldsymbol{v}_i = \boldsymbol{J}_i(\boldsymbol{q}_i)\boldsymbol{\zeta}_i,\ i \in \mathcal{K} \tag{1}$$

where $\boldsymbol{\zeta}_i = [\boldsymbol{\varpi}_i{}^\top, \dot{\boldsymbol{q}}_{m,i}^\top]^\top \in \mathbb{R}^{6+n}$ is the velocity vector involving the body velocities of the vehicle as well as the joint velocities of the manipulator with $\boldsymbol{\varpi}_i$ denoting the velocity of the vehicle expressed in the body-fixed frame and $\boldsymbol{J}_i(\boldsymbol{q}_i)$ denoting the Jacobian matrix [15]. Furthermore, owing to the rigid grasp of the object and since the object geometric parameters are considered known, it is straightforward to compute the object's position w.r.t the inertial frame $\{I\}$. Moreover, along with the fact that $\boldsymbol{\omega}_i = \boldsymbol{\omega}_O,\ i \in \mathcal{K}$, one obtains:

$$\boldsymbol{v}_i = \boldsymbol{J}_{iO}\boldsymbol{v}_O,\ i \in \mathcal{K} \tag{2}$$

where $\boldsymbol{J}_{iO},\ i \in \mathcal{K}$ denotes the Jacobian from the object frame to the end-effector frame of each UVMS, that is defined as:

$$\boldsymbol{J}_{iO} = \begin{bmatrix} \boldsymbol{I}_{3\times3} & -\boldsymbol{S}(\boldsymbol{l}_i) \\ \boldsymbol{0}_{3\times3} & \boldsymbol{I}_{3\times3} \end{bmatrix} \in \mathbb{R}^{6\times6},\quad i \in \mathcal{K} \tag{3}$$

where $\boldsymbol{S}(\boldsymbol{l}_i)$ is the skew-symmetric matrix of the constant relative position $\boldsymbol{l}_i = [l_{ix}, l_{iy}, l_{iz}]^\top$ of the end-effector w.r.t the object, expressed in the object's frame, defined as:

$$\boldsymbol{S}(\boldsymbol{l}_i) = \begin{bmatrix} 0 & -l_{iz} & l_{iy} \\ l_{iz} & 0 & -l_{ix} \\ -l_{iy} & l_{ix} & 0 \end{bmatrix} \in \mathbb{R}^{3\times3},\ i \in \mathcal{K}$$

Notice that $\boldsymbol{J}_{iO},\ i \in \mathcal{K}$ are always full-rank owing to the grasp rigidity and hence obtain a well defined inverse. Thus, the object's velocity can be easily computed via the inverse of (2). Moreover, from (2), one obtains the acceleration relation:

$$\dot{\boldsymbol{v}}_i = \boldsymbol{J}_{iO}\dot{\boldsymbol{v}}_O + \dot{\boldsymbol{J}}_{iO}\boldsymbol{v}_O,\ i \in \mathcal{K} \tag{4}$$

which will be used in the subsequent analysis.

B. Dynamics

UVMS Dynamics: The dynamics of a UVMS after straightforward algebraic manipulations can be written as [15]:

$$\begin{aligned}\boldsymbol{M}_{q_i}(\boldsymbol{q}_i)\dot{\boldsymbol{\zeta}}_i + \boldsymbol{C}_{q_i}(\boldsymbol{\zeta}_i, \boldsymbol{q}_i)\boldsymbol{\zeta}_i + \boldsymbol{D}_{q_i}(\boldsymbol{\zeta}_i, \boldsymbol{q}_i)\boldsymbol{\zeta}_i \\ + \boldsymbol{g}_{q_i}(\boldsymbol{q}_i) + \boldsymbol{d}_{q_i}(\boldsymbol{\zeta}_i, \boldsymbol{q}_i, t) = \boldsymbol{\tau}_i + \boldsymbol{J}_i{}^\top \boldsymbol{\lambda}_i\end{aligned} \tag{5}$$

for $i \in \mathcal{K}$, where $\boldsymbol{\lambda}_i$ is the vector of *measured* interaction forces and torques exerted on the end-effector by the object at end-effector frame, $\boldsymbol{\tau}_i$ denotes the vector of control inputs (forces and torques), $\boldsymbol{M}_{q_i}(\boldsymbol{q}_i)$ is the inertial matrix, $\boldsymbol{C}_{q_i}(\boldsymbol{\zeta}_i, \boldsymbol{q}_i)$ represents coriolis and centrifugal terms, $\boldsymbol{D}_{q_i}(\boldsymbol{\zeta}_i, \boldsymbol{q}_i)$ models dissipative effects, $\boldsymbol{g}_i(\boldsymbol{q}_i)$ encapsulates the gravity and buoyancy effects and $\boldsymbol{d}_{q_i}(\boldsymbol{\zeta}_i, \boldsymbol{q}_i, t)$ is a bounded vector representing unmodeled friction, uncertainties and external disturbances. In view of (1), we have:

$$\dot{\boldsymbol{v}}_i = \boldsymbol{J}_i(\boldsymbol{q}_i)\dot{\boldsymbol{\zeta}}_i + \boldsymbol{J}_i^d(\boldsymbol{\zeta}_i, \boldsymbol{q}_i)\boldsymbol{\zeta}_i,\ i \in \mathcal{K} \tag{6}$$

where $\boldsymbol{J}_i^d(\boldsymbol{\zeta}_i, \boldsymbol{q}_i) \in \mathbb{R}^{6\times(6+n)}$ represents the Jacobian derivative function (i.e., $\boldsymbol{J}_i^d(\boldsymbol{\zeta}_i, \boldsymbol{q}_i) \triangleq \dot{\boldsymbol{J}}_i(\boldsymbol{q}_i)$). Then, by employing the differential kinematics as well as (6), we obtain the transformed task space dynamics [64]:

$$\begin{aligned}\boldsymbol{M}_{v_i}(\boldsymbol{q}_i)\dot{\boldsymbol{v}}_i + \boldsymbol{C}_{v_i}(\boldsymbol{\zeta}_i, \boldsymbol{q}_i)\boldsymbol{v}_i + \boldsymbol{D}_{v_i}(\boldsymbol{\zeta}_i, \boldsymbol{q}_i)\boldsymbol{v}_i \\ + \boldsymbol{g}_{v_i}(\boldsymbol{q}_i) + \boldsymbol{d}_{v_i}(\boldsymbol{\zeta}_i, \boldsymbol{q}_i, t) = \boldsymbol{u}_i + \boldsymbol{\lambda}_i\end{aligned} \tag{7}$$

with $\boldsymbol{u}_i \in \mathbb{R}^6$ denoting the control vector of task space generalized forces/torques and the corresponding task space terms $\boldsymbol{M}_{v_i} \in \mathbb{R}^{6\times6}$, $\boldsymbol{C}_{v_i} \in \mathbb{R}^{6\times6}$, $\boldsymbol{D}_{v_i} \in \mathbb{R}^{6\times6}$, $\boldsymbol{g}_{v_i} \in \mathbb{R}^6$, $\boldsymbol{d}_{v_i} \in \mathbb{R}^6$ given as:

$$\begin{aligned}\boldsymbol{M}_i(\boldsymbol{q}_i) &= [\boldsymbol{J}_i(\boldsymbol{q}_i)\boldsymbol{M}_{q_i}^{-1}\boldsymbol{J}_i(\boldsymbol{q}_i)^\top]^{-1} \\ \boldsymbol{C}_i(\boldsymbol{\zeta}_i, \boldsymbol{q}_i)\boldsymbol{J}_i(\boldsymbol{q}_i)\boldsymbol{\zeta}_i &= \boldsymbol{M}_i(\boldsymbol{q}_i)\big[\boldsymbol{J}_i(\boldsymbol{q}_i)\boldsymbol{M}_{q_i}^{-1}\boldsymbol{C}_{q_i} - \dot{\boldsymbol{J}}_i(\boldsymbol{q}_i)\big]\boldsymbol{\zeta}_i \\ \boldsymbol{D}_i(\boldsymbol{\zeta}_i, \boldsymbol{q}_i)\boldsymbol{J}_i(\boldsymbol{q}_i)\boldsymbol{\zeta}_i &= \boldsymbol{M}_i(\boldsymbol{q}_i)\boldsymbol{J}_i(\boldsymbol{q}_i)\boldsymbol{M}_{q_i}^{-1}\boldsymbol{D}_{q_i}\boldsymbol{\zeta}_i \\ \boldsymbol{g}_i(\boldsymbol{q}_i) &= \boldsymbol{M}_i(\boldsymbol{q}_i)\boldsymbol{J}_i(\boldsymbol{q}_i)\boldsymbol{M}_{q_i}^{-1}\boldsymbol{g}_{q_i} \\ \boldsymbol{d}_i(\boldsymbol{\zeta}_i, \boldsymbol{q}_i, t) &= \boldsymbol{M}_i(\boldsymbol{q}_i)\boldsymbol{J}_i(\boldsymbol{q}_i)\boldsymbol{M}_{q_i}^{-1}\boldsymbol{d}_{q_i}\end{aligned}$$

Remark 1: It is worth noting that the vector of control inputs $\boldsymbol{\tau}_i,\ i \in \mathcal{K}$ can be related to the task space wrench $\boldsymbol{u}_i \in \mathbb{R}^6,\ i \in \mathcal{K}$ via:

$$\boldsymbol{\tau}_i = \boldsymbol{J}_i^\top(\boldsymbol{q}_i)\boldsymbol{u}_i + (\boldsymbol{I}_{6+n} - \boldsymbol{J}_i^\top(\boldsymbol{q}_i)\tilde{\boldsymbol{J}}_i^\top(\boldsymbol{q}_i))\boldsymbol{\tau}_{i0} \tag{8}$$

where $\tilde{\boldsymbol{J}}_i^\top(\boldsymbol{q}_i)$ is the generalized pseudo-inverse of $\boldsymbol{J}_i$ [64] and the vector $\boldsymbol{\tau}_{i0}$ does not contribute to the end effector's wrench $\boldsymbol{u}_i$, since it belongs to the null space of the Jacobian $\boldsymbol{J}_i$ and thus can be regulated independently to achieve secondary tasks (e.g., maintaining manipulator's joint limits or increasing the manipulability)[4]. Please note that the aforementioned potential secondary tasks should be developted in a dynamic level, instead than in a kinematic level as it is commonly done.

Invoking the kinematic relations (2)-(4), we may express the aforementioned dynamics (7) with respect to the object's coordinates as follows:

$$\begin{aligned}\boldsymbol{M}_i(\boldsymbol{q}_i)\dot{\boldsymbol{v}}_O + \boldsymbol{C}_i(\boldsymbol{\zeta}_i, \boldsymbol{q}_i)\boldsymbol{v}_O + \boldsymbol{D}_i(\boldsymbol{\zeta}_i, \boldsymbol{q}_i)\boldsymbol{v}_O \\ + \boldsymbol{g}_i(\boldsymbol{q}_i) + \boldsymbol{d}_i(\boldsymbol{\zeta}_i, \boldsymbol{q}_i, t) = \boldsymbol{J}_{iO}^\top\boldsymbol{u}_i + \boldsymbol{J}_{iO}^\top\boldsymbol{\lambda}_i\end{aligned} \tag{9}$$

where

$$\begin{aligned}\boldsymbol{M}_i(\boldsymbol{q}_i) &= \boldsymbol{J}_{iO}^\top\boldsymbol{M}_{v_i}(\boldsymbol{q}_i)\boldsymbol{J}_{iO} \\ \boldsymbol{C}_i(\boldsymbol{\zeta}_i, \boldsymbol{q}_i) &= \boldsymbol{J}_{iO}^\top\big[\boldsymbol{C}_{v_i}(\boldsymbol{\zeta}_i, \boldsymbol{q}_i)\boldsymbol{J}_{iO} + \boldsymbol{M}_{v_i}(\boldsymbol{q}_i)\dot{\boldsymbol{J}}_{iO}\big] \\ \boldsymbol{D}_i(\boldsymbol{\zeta}_i, \boldsymbol{q}_i) &= \boldsymbol{J}_{iO}^\top\boldsymbol{D}_{v_i}(\boldsymbol{\zeta}_i, \boldsymbol{q}_i)\boldsymbol{J}_{iO} \\ \boldsymbol{g}_i(\boldsymbol{q}_i) &= \boldsymbol{J}_{iO}^\top\boldsymbol{g}_{v_i}(\boldsymbol{q}_i) \\ \boldsymbol{d}_i(\boldsymbol{\zeta}_i, \boldsymbol{q}_i, t) &= \boldsymbol{J}_{iO}^\top\boldsymbol{d}_{v_i}(\boldsymbol{\zeta}_i, \boldsymbol{q}_i, t)\end{aligned}$$

Now, the following common properties will be employed in the analysis.

[4] For more details on task priority based control and redundancy resolution for mobile manipulators the reader is referred to [58], [65] and [66], [67].

***Property** 1:* The matrix $\boldsymbol{M}_i(\boldsymbol{q}_i),\ i \in \mathcal{K}$ is positive definite and the matrix $\dot{\boldsymbol{M}}_i(\boldsymbol{q}_i) - 2\boldsymbol{C}_i(\boldsymbol{\zeta}_i, \boldsymbol{q}_i),\ i \in \mathcal{K}$ is skew-symmetric.

***Property** 2:* The uncertainty of the UVMS model appears linearly in the dynamics (9) in terms of an unknown but constant parameter vector $\boldsymbol{\theta}_i \in \mathbb{R}^{q_i},\ i \in \mathcal{K}$ in the following formulation [68], [69]:

$$\begin{aligned}\boldsymbol{M}_i(\boldsymbol{a}_i)\boldsymbol{d}_i + \boldsymbol{C}_i(\boldsymbol{a}_i, \boldsymbol{b}_i)\boldsymbol{c}_i + \boldsymbol{D}_i(\boldsymbol{a}_i, \boldsymbol{b}_i)\boldsymbol{c}_i + \boldsymbol{g}_i(\boldsymbol{a}_i) \\ = \boldsymbol{\Omega}_i(\boldsymbol{a}_i, \boldsymbol{b}_i, \boldsymbol{c}_i, \boldsymbol{d}_i)\boldsymbol{\theta}_i,\ i \in \mathcal{K}\end{aligned} \tag{10}$$

where $\boldsymbol{\Omega}_i(\boldsymbol{a}_i, \boldsymbol{b}_i, \boldsymbol{c}_i, \boldsymbol{d}_i) \in \mathbb{R}^{6\times q_i},\ i \in \mathcal{K}$ is a regressor matrix of known functions of $\boldsymbol{a}_i, \boldsymbol{b}_i, \boldsymbol{c}_i, \boldsymbol{d}_i \in \mathbb{R}^6$ independent of $\boldsymbol{\theta}_i$. Now, we introduce the following assumption regarding the unmodeled dynamics/external disturbances.

Assumption 1: There exist unknown constant vector $\boldsymbol{\theta}_{d,i} \in \mathbb{R}^{q_i}$ and known bounded functions $\boldsymbol{\Delta}_i \in \mathbb{R}^{6\times q_i}$, such that

$$\boldsymbol{d}_i(\boldsymbol{\zeta}_i, \boldsymbol{q}_i, t) = \boldsymbol{\Delta}_i(\boldsymbol{\zeta}_i, \boldsymbol{q}_i, t)\boldsymbol{\theta}_{d,i},\ i \in \mathcal{K}. \tag{11}$$

Object Dynamics: Without any loss of generality, we consider the following second order dynamics for the object, which can be derived based on the Newton-Euler formulation:

$$\dot{\boldsymbol{x}}_O = \boldsymbol{J}_O(\boldsymbol{\eta}_{2,O})\boldsymbol{v}_O \tag{12a}$$

$$\boldsymbol{M}_O(\boldsymbol{x}_O)\dot{\boldsymbol{v}}_O + \boldsymbol{C}_O(\dot{\boldsymbol{x}}_O, \boldsymbol{x}_O)\boldsymbol{v}_O + \boldsymbol{D}_O(\dot{\boldsymbol{x}}_O, \boldsymbol{x}_O)\boldsymbol{v}_O + \boldsymbol{g}_O = \boldsymbol{\lambda}_O + \boldsymbol{\lambda}_e \tag{12b}$$

where $\boldsymbol{x}_O = [\boldsymbol{\eta}_{1,O}^\top, \boldsymbol{\eta}_{2,O}^\top]^\top$ denotes the task space coordinates of the commonly agreed body-fixed frame on the object, $\boldsymbol{M}_O(\boldsymbol{x}_O)$ is the positive definite inertia matrix, $\boldsymbol{C}_O(\dot{\boldsymbol{x}}_O, \boldsymbol{x}_O)$ is the Coriolis matrix, $\boldsymbol{g}_O$ is the vector of gravity and buoyancy effects, $\boldsymbol{D}_O(\dot{\boldsymbol{x}}_O, \boldsymbol{x}_O)$ models dissipative effects, $\boldsymbol{\lambda}_O$ is the vector of generalized forces acting on the object's center of mass, $\boldsymbol{\lambda}_e$ is a vector representing uncertainties and external disturbances and $\boldsymbol{J}_O(\boldsymbol{\eta}_{2,O}) = \text{diag}\{\boldsymbol{I}_3, \boldsymbol{J}'_O(\boldsymbol{\eta}_{2,O})\}$ is the object representation Jacobian with:

$$\boldsymbol{J}'_O(\boldsymbol{\eta}_{2,O}) = \begin{bmatrix} 1 & \sin(\phi_O)\tan(\theta_O) & cos(\phi_O)\tan(\theta_O) \\ 0 & \cos(\phi_O) & -\sin(\theta_O) \\ 0 & \frac{\sin(\phi_O)}{\cos(\theta_O)} & \frac{cos(\phi_O)}{\cos(\theta_O)} \end{bmatrix} \tag{13}$$

Moreover, the kineto-statics duality along with the grasp rigidity suggest that the force $\boldsymbol{\lambda}_O$ acting on the object's center of mass and the generalized forces $\boldsymbol{\lambda}_i,\ i \in \mathcal{K}$, exerted by the UVMSs at the grasping points, are related through:

$$\boldsymbol{\lambda}_O = \boldsymbol{G}^\top \boldsymbol{\lambda} \tag{14}$$

where

$$\boldsymbol{G} = \left[[\boldsymbol{J}_{LO}]^\top, [\boldsymbol{J}_{F_1O}]^\top, \ldots, [\boldsymbol{J}_{F_NO}]^\top\right]^\top \in \mathbb{R}^{6(N+1)\times 6} \tag{15}$$

is the full column-rank grasp matrix and $\boldsymbol{\lambda} = [\boldsymbol{\lambda}_{\boldsymbol{L}}^\top, \boldsymbol{\lambda}_{\boldsymbol{F_1}}^\top, \ldots, \boldsymbol{\lambda}_{\boldsymbol{F_N}}^\top]^\top$ is the vector of the overall interaction forces and torques.

Remark 2: Wrenches that lie on the null space of the grasp matrix $\boldsymbol{G}^\top$ do not contribute to the object dynamics. Therefore, we may incorporate in the control scheme an extra component $\boldsymbol{\lambda}_{int,i} = (\boldsymbol{I} - (\boldsymbol{G}^\top)^{\#}\boldsymbol{G}^\top)\boldsymbol{\lambda}_{int}^d,\ i \in \mathcal{K}$, that belongs to the null space of $\boldsymbol{G}^\top$, in order to regulate the steady state internal forces, where $(\boldsymbol{G}^\top)^{\#}$ denotes the generalized inverse of $\boldsymbol{G}^\top$. Notice that owing to the rigid grasp, $l_i,\ i \in \mathcal{K}$ remain constant, thus, if $\boldsymbol{\lambda}_{int}^d$ is chosen constant, and $l_i,\ i \in \mathcal{K}$ are considered known to the team of UVMSs,[5] no communication is needed to compute $\boldsymbol{G}^\top$, $(\boldsymbol{G}^\top)^{\#}$ and $\boldsymbol{\lambda}_{int,i}$ during task execution.

C. Description of the Workspace

Consider the team of $N+1$ UVMSs operating in a bounded workspace $\mathcal{W} \subseteq \mathbb{R}^3$ with boundary $\partial\mathcal{W}$. The object of interest is a rigid body which is required to be transported cooperatively by the robot team from an initial to a goal position. Without any loss of the generality, the obstacles, the robots as well as the workspace are all modeled by spheres (i.e., we adopt the spherical world representation [70]). However, the proposed control strategy could be extended to more general and complex geometries following the analysis in [70]. In this spirit, let $\mathcal{B}(\boldsymbol{x}_O, r_0)$ be a closed ball that covers the volume of the object and has radius r_0. We also define the closed balls $\mathcal{B}(\boldsymbol{x}_i, \bar{r}), i \in \mathcal{K}$, centered at the end-effector of each UVMS that cover the robot volume for all possible configurations. Notice that the value of $\bar{r}$ can be calculated easily for each UVMS based solely on its own design parameters. We also select the distance among the grasping points on the given object to be at least $2\bar{r}$. In particular, the distance $2\bar{r}$ denotes the minimum allowed distance at which two bounding spheres $\mathcal{B}(\boldsymbol{x}_i, \bar{r})$ and $\mathcal{B}(\boldsymbol{x}_j, \bar{r})$ $i, j \in \mathcal{K}, i \neq j$ do not collide (see Fig. 2). Furthermore, we define a ball area $\mathcal{B}(\boldsymbol{x}_O, R)$ located at

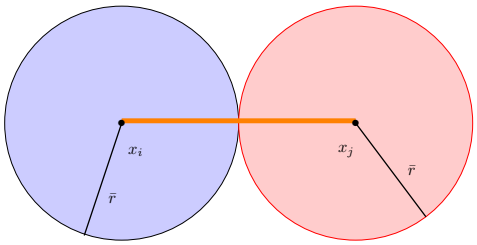

Fig. 2. Graphical representation of the minimum allowed distance $\bar{r}$.

$\boldsymbol{x}_O$ with radius $R = \bar{r} + r_o$ that includes the whole volume of the robotic team and the object (see Fig. 3). Finally, the $\mathcal{M}$ static obstacles within the workspace are defined as closed spheres described by $\pi_m = \mathcal{B}(\boldsymbol{p}_{\pi_m}, r_{\pi_m}),\ m \in \{1, \ldots, \mathcal{M}\}$, where $\boldsymbol{p}_{\pi_m} \in \mathbb{R}^3$ is the center and the $r_{\pi_m} > 0$ is the radius of the obstacle π_m. Obviously, the ultimate goal of the proposed cooperative control strategy is to transport the object from the initial configuration to the desired one, without colliding with the obstacles and the boundary of the workspace. Additionally, based on the property of spherical world [70], for each pair of obstacles $m, m' \in \{1, \ldots, \mathcal{M}\}$ the following inequality holds:

$$||\boldsymbol{p}_{\pi_m} - \boldsymbol{p}_{\pi'_m}|| > 2R + r_{\pi_m} + r_{\pi'_m} \tag{16}$$

which intuitively means that two obstacles are disjoint in such a way that the whole team of UVMSs including the object can pass through the free space between them. Therefore, there exists a feasible trajectory $\boldsymbol{x}_O(t)$ for the whole team

[5]This can be achieved by using the acoustic modems before initialing the task execution.

that connects the initial configuration $\boldsymbol{x}_O(t_0)$ with $\boldsymbol{x}_O^d$ such that:

$$\mathcal{B}(\boldsymbol{x}_O(t), R) \cap \{\mathcal{B}(\boldsymbol{p}_{\pi_m}, r_{\pi_m}) \cup \partial\mathcal{W}\} = \emptyset, \ \forall m \in \{1, \ldots, \mathcal{M}\} \quad (17)$$

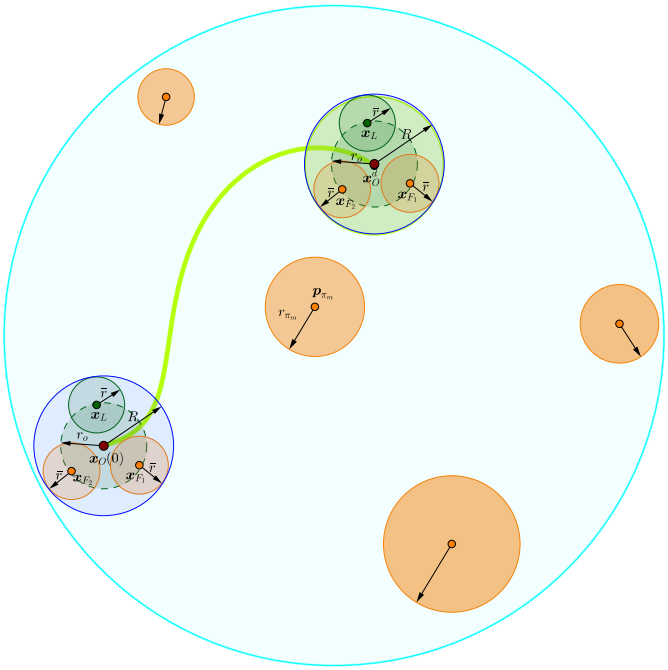

Fig. 3. Graphical representation of a feasible trajectory of the team of UVMS carrying object from the initial position $\boldsymbol{x}_O(t_0)$ to the desired position $\boldsymbol{x}_O^d$. The boundary of workspace $\partial\mathcal{W}$ is illustrated in cyan. Red circles indicate the obstacles within the workspace $\mathcal{W}$. A feasible trajectory of the whole team is depicted in green.

Hence, the problem that we aim to solve in this paper is stated as follows.

Problem: Given $N+1$ UVMSs operating in a constrained workspace $\mathcal{W}$, design distributed control protocols $\boldsymbol{u}_i$, $i \in \mathcal{K}$ that navigate safely the whole robotic team to the desired configuration without colliding with the obstacles and the boundary of the workspace, while satisfying the following specifications: i) Impose no strict requirements regarding the underwater communication bandwidth; and ii)Enforce robustness against the parametric uncertainty of the UVMS dynamic model.

III. Control Methodology

We assume that the leading UVMS is aware of both the desired configuration of the object as well as of the obstacles' position in the workspace. Thus, its control objective is to navigate the overall formation towards the goal configuration while avoiding collisions with the static obstacles. Towards this direction and in view of (17), we assume that there is a feasible trajectory within the workspace which is known only to the leader. On the other hand, the followers are not aware of the object's desired trajectory. However, even though explicit inter-robot communication is not permitted, the followers will estimate the object's desired trajectory profile via their own state measurements. Towards this direction, acceleration residuals owing to the lack of acceleration measurements for the object will be compensated by adopting a robust prescribed performance estimator that guarantees ultimate boundedness of the estimation error with predefined transient and steady state specifications. Finally, appropriate adaptive laws will be designed to achieve the asymptotic tracking of the estimated trajectory profile, thus increasing the robustness of the overall control scheme and avoiding high interaction forces among the object and the robots.

A. Control Design

In the sequel, we propose a distributed control scheme that guarantees the asymptotic stabilization of the object to the goal configuration $\boldsymbol{x}_O^d$. Before proceeding with the analysis, we introduce the load sharing coefficients c_i, $i \in \mathcal{K}$ that are subject to the following design constraints:

$$c_i \in (0,1), \forall i \in \mathcal{K} \text{ and } \sum_{i \in \mathcal{K}} c_i = 1. \quad (18)$$

Without any loss of generality and to simplify the analysis we select:

$$c_i = \frac{1}{N+1}, \qquad i \in \mathcal{K}. \quad (19)$$

Based on the load coefficients (19) the object dynamics of (12b) can be rewritten as:

$$\sum_{i \in \mathcal{K}} \{\boldsymbol{M}_{O_i}(\boldsymbol{x}_O)\dot{\boldsymbol{v}}_O + \boldsymbol{C}_{O_i}(\dot{\boldsymbol{x}}_O, \boldsymbol{x}_O)\boldsymbol{v}_O + \boldsymbol{D}_{O_i}(\dot{\boldsymbol{x}}_O, \boldsymbol{x}_O)\boldsymbol{v}_O + \boldsymbol{g}_{O_i}\}$$
$$= \sum_{i \in \mathcal{K}} \boldsymbol{J}_{iO}^{\top} \boldsymbol{\lambda}_i + \sum_{i \in \mathcal{K}} \boldsymbol{\lambda}_{e_i} \quad (20)$$

where $\boldsymbol{M}_{O_i} = c_i \boldsymbol{M}_O$, $\boldsymbol{C}_{O_i} = c_i \boldsymbol{C}_O$, $\boldsymbol{D}_{O_i} = c_i \boldsymbol{D}_O$, $\boldsymbol{g}_{O_i} = c_i \boldsymbol{g}_O$ and $\boldsymbol{\lambda}_{e_i} = c_i \boldsymbol{\lambda}_e$. Notice that the latter will be identified locally through an online low pass filter given in Section-III-D. Now let us assume that each UVMS is expected to exert the following desired force/torque on the object:

$$\boldsymbol{\lambda}_i^d = \boldsymbol{\lambda}_{int,i}^d - \boldsymbol{J}_{iO}^{-\top}(\boldsymbol{M}_{O_i}\boldsymbol{y}_i^{cmd} + \boldsymbol{C}_{O_i}\boldsymbol{v}_O + \boldsymbol{D}_{O_i}\boldsymbol{v}_O + \boldsymbol{g}_{O_i} - \boldsymbol{\lambda}_{e_i}) \quad (21)$$

where $\boldsymbol{\lambda}_{int,i}^d$ denotes the desired internal forces (see Remark 2) and $\boldsymbol{y}_i^{cmd}$ is a pre-designed input given by:

$$\boldsymbol{y}_i^{cmd} = \dot{\boldsymbol{v}}_{O_i}^d + \boldsymbol{M}_{d_O}^{-1}\left[-\boldsymbol{D}_{d_O}\tilde{\boldsymbol{v}}_{O_i} - \boldsymbol{K}_{d_O}\tilde{\boldsymbol{e}}_{O_i}\right] \quad (22)$$

where $\boldsymbol{M}_{d_O}$, $\boldsymbol{D}_{d_O}$ and $\boldsymbol{K}_{d_O}$ are the desired inertia, damping and stiffness matrices for the object dynamics, $\tilde{\boldsymbol{v}}_{O_i}(t) = \boldsymbol{v}_O - \boldsymbol{v}_{O_i}^d$ denotes the velocity error and $\tilde{\boldsymbol{e}}_{O_i}$ is the object pose error, defined as:

$$\tilde{\boldsymbol{e}}_{O_i} = \begin{bmatrix} \boldsymbol{\eta}_{1,O} - \boldsymbol{\eta}_{1,O_i}^d \\ \tilde{\boldsymbol{\epsilon}}_{O_i} \end{bmatrix} \quad (23)$$

where

$$\tilde{\boldsymbol{\epsilon}}_{O_i} = \frac{1}{2}\left(\boldsymbol{n}_O \times \boldsymbol{n}_{O_i}^d + \boldsymbol{o}_O \times \boldsymbol{o}_{O_i}^d + \boldsymbol{\alpha}_O \times \boldsymbol{\alpha}_{O_i}^d\right) \in \mathbb{R}^3 \quad (24)$$

is the orientation error expressed in the outer product formulation [71]. Notice that for the orientation error $\tilde{\boldsymbol{\epsilon}}_{O_i}$ we employed the outer product formulation [71] of the rotation matrix $\boldsymbol{R}_O = [\boldsymbol{n}_O, \boldsymbol{o}_O, \boldsymbol{\alpha}_O]$ and the desired rotation matrix $\boldsymbol{R}_{O_i}^d = [\boldsymbol{n}_{O_i}^d, \boldsymbol{o}_{O_i}^d, \boldsymbol{\alpha}_{O_i}^d]$ which also relaxes the representation

singularity issue that is inherent in case of Euler angles. In view of (20), it can be concluded that if all robots cooperatively apply the desired wrench vector (21) to the object, then

$$\boldsymbol{M}_{d_O}\dot{\tilde{\boldsymbol{v}}}_O + \boldsymbol{D}_{d_O}\tilde{\boldsymbol{v}}_O + \boldsymbol{K}_{d_O}\tilde{\boldsymbol{e}}_O = \boldsymbol{0} \tag{25}$$

which intuitively means that the aforementioned selection of $\boldsymbol{\lambda}_i^d$ cancels the object's nonlinearities, ensures adequate internal forces via $\boldsymbol{\lambda}_{int,i}^d$ and achieves the desired dynamics of the object defined by the desired impedance behavior which is described by the the desired inertia, damping and stiffness matrices $\boldsymbol{M}_{d_o},\ \boldsymbol{D}_{d_o}, \boldsymbol{K}_{d_o}$ respectively [72]. Thus, the control objective for each UVMS $i \in \mathcal{K}$ is to enforce $\lim_{t\to\infty} \boldsymbol{w}_i(t) = 0$, where the error signal $\boldsymbol{w}(t)$ is constructed as:

$$\boldsymbol{w}_i(t) = \boldsymbol{M}_d\dot{\tilde{\boldsymbol{v}}}_{O_i} + \boldsymbol{D}_d\tilde{\boldsymbol{v}}_{O_i} + \boldsymbol{K}_d\tilde{\boldsymbol{e}}_{O_i} - \boldsymbol{J}_{iO}^{\top}\boldsymbol{\lambda}_i^d,\ i \in \mathcal{K} \tag{26}$$

where $\boldsymbol{M}_d$, $\boldsymbol{D}_d$ and $\boldsymbol{K}_d$ are the desired inertia, damping and stiffness matrices for the robot dynamics.

Remark 3: The (25) describes the desired impedance behavior for the object dynamics while the (26) describes the desired behavior for each robot dynamics. More specifically, in view of (20), as it is stated before, we have that if all robots cooperatively apply the desired wrench vector (21) to the object, it yields the desired behavior of the object dynamics given in (25). That consequently results into tracking the object desired trajectory with a predefined desired behavior given in (25). We now seek to force each robot to apply the aforementioned desired wrench vector of (21) to the object. In order to achieve that, the error $\boldsymbol{w}_i(t)$ is constructed for each robots as it is given in (26). Therefore, the control objective for each robots is $\lim_{t\to\infty} \boldsymbol{w}_i(t) = 0$ which results in applying the desired wrench vector of (21) to the object with a predefined and desired impedance behavior which is described in (26) by the desired inertia, damping and stiffness matrices $\boldsymbol{M}_d,\ \boldsymbol{D}_d, \boldsymbol{K}_d$ respectively. Notice that here for the sake of simplicity, we have set that all robots have the same impedance desired behavior matrices. However, considering different desired behavior matrices affects only the convergence rate and not the stability properties of the system.

Now, in view of (26) we get an augmented impedance error:

$$\tilde{\boldsymbol{w}}_i = \boldsymbol{K}_f\boldsymbol{w}_i = \dot{\tilde{\boldsymbol{v}}}_{O_i} + \boldsymbol{K}_g\tilde{\boldsymbol{v}}_{O_i} + \boldsymbol{K}_p\tilde{\boldsymbol{e}}_{O_i} - \boldsymbol{K}_f\boldsymbol{J}_{iO}^{\top}\boldsymbol{\lambda}_i^d \tag{27}$$

where $\boldsymbol{K}_f = \boldsymbol{M}_d^{-1}$, $\boldsymbol{K}_g = \boldsymbol{K}_f\boldsymbol{D}_d$, and $\boldsymbol{K}_p = \boldsymbol{K}_f\boldsymbol{K}_d$. We also choose two positive-definite matrices $\boldsymbol{F}$ and $\boldsymbol{Y}$ such that:

$$\boldsymbol{F} + \boldsymbol{Y} = \boldsymbol{K}_g \tag{28a}$$

$$\dot{\boldsymbol{F}} + \boldsymbol{Y}\boldsymbol{F} = \boldsymbol{K}_p \tag{28b}$$

and define the filtered force/torque measurement:

$$\dot{\boldsymbol{f}}_i + \boldsymbol{Y}\boldsymbol{f}_i = \boldsymbol{K}_f\boldsymbol{J}_{iO}^{\top}\boldsymbol{\lambda}_i^d,\ i \in \mathcal{K}. \tag{29}$$

Thus, we may rewrite (27) as:

$$\tilde{\boldsymbol{w}}_i = \dot{\tilde{\boldsymbol{v}}}_{O_i} + (\boldsymbol{F}+\boldsymbol{Y})\tilde{\boldsymbol{v}}_{O_i} + (\dot{\boldsymbol{F}}+\boldsymbol{Y}\boldsymbol{F})\tilde{\boldsymbol{e}}_{O_i} - \dot{\boldsymbol{f}}_i - \boldsymbol{Y}\boldsymbol{f}_i. \tag{30}$$

Now we define the auxiliary variables $\boldsymbol{z}_i,\ i \in \mathcal{K}$ as:

$$\boldsymbol{z}_i = \tilde{\boldsymbol{v}}_{O_i} + \boldsymbol{F}\tilde{\boldsymbol{e}}_{O_i} - \boldsymbol{f}_i,\ i \in \mathcal{K}. \tag{31}$$

Hence, the augmented impedance error becomes:

$$\tilde{\boldsymbol{w}}_i = \dot{\boldsymbol{z}}_i + \boldsymbol{Y}\boldsymbol{z}_i,\ i \in \mathcal{K} \tag{32}$$

which represents a stable low pass filter. Therefore, if we achieve $\lim_{t\to\infty} \boldsymbol{z}_i(t) = 0$, then the initial control objective is readily met, i.e, $\lim_{t\to\infty} \boldsymbol{w}_i(t) = 0$. In this respect, let us define the augmented state variable:

$$\boldsymbol{v}_{O_i}^r = \boldsymbol{v}_{O_i}^d - \boldsymbol{F}\tilde{\boldsymbol{e}}_{O_i} + \boldsymbol{f}_i,\ i \in \mathcal{K} \tag{33}$$

Thus, (31) and (33) immediately result in:

$$\boldsymbol{z}_i = \boldsymbol{v}_O - \boldsymbol{v}_{O_i}^r,\ i \in \mathcal{K} \tag{34}$$

from which the dynamics (9) becomes:

$$\begin{aligned}\boldsymbol{M}_i\dot{\boldsymbol{z}}_i + \boldsymbol{C}_i\boldsymbol{z}_i + \boldsymbol{D}_i\boldsymbol{z}_i = \boldsymbol{J}_{iO}^{\top}\boldsymbol{u}_i + \boldsymbol{J}_{iO}^{\top}\boldsymbol{\lambda}_i \\ -\Big[\boldsymbol{M}_i\dot{\boldsymbol{v}}_{O_i}^r + \boldsymbol{C}_i\boldsymbol{v}_{O_i}^r + \boldsymbol{D}_i\boldsymbol{v}_{O_i}^r + \boldsymbol{g}_i + \boldsymbol{d}_i\Big].\end{aligned} \tag{35}$$

Invoking Property 2 and Assumption 1 , we arrive at the open loop dynamics:

$$\begin{aligned}\boldsymbol{M}_i\dot{\boldsymbol{z}}_i + \boldsymbol{C}_i\boldsymbol{z}_i + \boldsymbol{D}_i\boldsymbol{z}_i = \boldsymbol{J}_{iO}^{\top}\boldsymbol{u}_i + \boldsymbol{J}_{iO}^{\top}\boldsymbol{\lambda}_i \\ -\boldsymbol{\Delta}_i(\boldsymbol{\zeta}_i, \boldsymbol{q}_i, t)\boldsymbol{\theta}_{d,i} - \boldsymbol{\Omega}_i(\boldsymbol{q}_i, \boldsymbol{\zeta}_i, \boldsymbol{v}_{O_i}^r, \dot{\boldsymbol{v}}_{O_i}^r)\boldsymbol{\theta}_i,\ i \in \mathcal{K}.\end{aligned} \tag{36}$$

Therefore, we design the following impedance control scheme:

$$\begin{aligned}\boldsymbol{u}_i = -\boldsymbol{\lambda}_i + \boldsymbol{J}_{iO}^{-\top}\Big[\boldsymbol{\Omega}_i(\boldsymbol{q}_i, \boldsymbol{\zeta}_i, \boldsymbol{v}_{O_i}^r, \dot{\boldsymbol{v}}_{O_i}^r)\hat{\boldsymbol{\theta}}_i \\ +\boldsymbol{\Delta}_i(\boldsymbol{\zeta}_i, \boldsymbol{q}_i, t)\hat{\boldsymbol{\theta}}_{d,i} - \boldsymbol{K}\boldsymbol{z}_i\Big],\ i \in \mathcal{K}\end{aligned} \tag{37}$$

where $\boldsymbol{K} > 0$ is a positive definite gain matrix and $\hat{\boldsymbol{\theta}}_i$, $\hat{\boldsymbol{\theta}}_{d,i}$ denote the estimates of the unknown parameters $\boldsymbol{\theta}_i$, $\boldsymbol{\theta}_{d,i}$ respectively, provided by the update laws:

$$\dot{\hat{\boldsymbol{\theta}}}_i = -\boldsymbol{\Gamma}_i\boldsymbol{\Omega}_i(\boldsymbol{q}_i, \boldsymbol{\zeta}_i, \boldsymbol{v}_{O_i}^r, \dot{\boldsymbol{v}}_{O_i}^r)\boldsymbol{z}_i,\ \boldsymbol{\Gamma}_i > 0 \tag{38}$$

$$\dot{\hat{\boldsymbol{\theta}}}_{d,i} = -\boldsymbol{\Gamma}_{d_i}\boldsymbol{\Delta}_i(\boldsymbol{\zeta}_i, \boldsymbol{q}_i, t)\boldsymbol{z}_i,\ \boldsymbol{\Gamma}_{d_i} > 0 \tag{39}$$

with $\boldsymbol{\Gamma}_i$, $\boldsymbol{\Gamma}_{d_i}$ positive diagonal gain matrices.

Theorem 1: Consider $N+1$ UVMSs that operate in a constrained workspace $\mathcal{W}$, with dynamics (9) obeying Properties 1–2; Assumption 1, and grasp rigidly a common object. The control scheme (37) with adaptive laws (38)-(39) guarantees $\lim_{t\to\infty} \boldsymbol{w}_i(t) = 0$ as well as the boundedness of all signals in the closed loop system.

Proof: Consider the following Lyapunov function candidate:

$$\boldsymbol{V} = \sum_{i\in\mathcal{K}}\frac{1}{2}\boldsymbol{z}_i^{\top}\boldsymbol{M}_i\boldsymbol{z}_i + \sum_{i\in\mathcal{K}}\frac{1}{2}\tilde{\boldsymbol{\theta}}_i^{\top}\boldsymbol{\Gamma}_i^{-1}\tilde{\boldsymbol{\theta}}_i + \sum_{i\in\mathcal{K}}\frac{1}{2}\tilde{\boldsymbol{\theta}}_{d_i}^{\top}\boldsymbol{\Gamma}_{d_i}^{-1}\tilde{\boldsymbol{\theta}}_{d_i} \tag{40}$$

where $\tilde{\boldsymbol{\theta}}_i = \hat{\boldsymbol{\theta}}_i - \boldsymbol{\theta}_i$ and $\tilde{\boldsymbol{\theta}}_{d_i} = \hat{\boldsymbol{\theta}}_{d_i} - \boldsymbol{\theta}_{d_i}$ denote the parametric errors. Differentiating with respect to time yields:

$$\dot{\boldsymbol{V}} = \sum_{i\in\mathcal{K}}\frac{1}{2}\boldsymbol{z}_i^{\top}\dot{\boldsymbol{M}}_i\boldsymbol{z}_i + \sum_{i\in\mathcal{K}}\boldsymbol{z}_i^{\top}\boldsymbol{M}_i\dot{\boldsymbol{z}}_i + \sum_{i\in\mathcal{K}}\tilde{\boldsymbol{\theta}}_i^{\top}\boldsymbol{\Gamma}_i^{\top}\dot{\hat{\boldsymbol{\theta}}}_i + \sum_{i\in\mathcal{K}}\tilde{\boldsymbol{\theta}}_{d_i}^{\top}\boldsymbol{\Gamma}_{d_i}^{\top}\dot{\hat{\boldsymbol{\theta}}}_{d_i}. \tag{41}$$

Invoking Property 1 and substituting the control scheme (37)-(39), we get:

$$\dot{\boldsymbol{V}} = \sum_{i\in\mathcal{K}} -\boldsymbol{z}_i^{\top}\boldsymbol{K}\boldsymbol{z}_i - \boldsymbol{z}_i^{\top}\boldsymbol{D}_i\boldsymbol{z}_i \leq \boldsymbol{0} \tag{42}$$

Hence, we conclude that $\boldsymbol{z}_i, \tilde{\boldsymbol{\theta}}_i, \tilde{\boldsymbol{\theta}}_{d_i} \in L_\infty$. Moreover, from the definition of $\boldsymbol{z}_i$ in (34), we also deduce that $\boldsymbol{x}_O, \boldsymbol{v}_O \in L_\infty$, and consequently $\boldsymbol{v}_{O_i}^r, \dot{\boldsymbol{v}}_{O_i}^r \in L_\infty$. Furthermore, employing (36) we arrive at $\dot{\boldsymbol{z}} \in L_\infty$. Therefore, integrating both sides of (42) leads to:

$$\boldsymbol{V}(t)-\boldsymbol{V}(0) \leq \sum_{i\in\mathcal{K}} \int_0^t \Big(-\boldsymbol{z}_i^\top(\tau)\boldsymbol{K}\boldsymbol{z}_i - \boldsymbol{z}_i^\top \boldsymbol{D}_i \boldsymbol{z}_i(\tau)\Big) d\tau \quad (43)$$

Thus, $\int_0^t \big(-\boldsymbol{z}_i^\top(\tau)\boldsymbol{K}\boldsymbol{z}_i - \boldsymbol{z}_i^\top \boldsymbol{D}_i \boldsymbol{z}_i(\tau)\big) d\tau$ is bounded, which results in $\boldsymbol{z}_i \in L_2$. Finally, applying Barbalat's Lemma and invoking (32) we get $\lim_{t\to\infty} \boldsymbol{w}_i(t) \to \boldsymbol{0},\ \forall i \in \mathcal{K}$, which completes the proof.

B. Safe Navigation

The desired/feasible object trajectory within the workspace $\mathcal{W}$ can be generated based on the Navigation Functions concept originally proposed by Rimon and Koditschek in [70], as follows:

$$\phi_O(\boldsymbol{x}_O; \boldsymbol{x}_O^d) = \frac{\gamma(\boldsymbol{x}_O - \boldsymbol{x}_O^d)}{\big[\gamma^k(\boldsymbol{x}_O - \boldsymbol{x}_O^d) + \beta(\boldsymbol{x}_O)\big]^{\frac{1}{k}}} \quad (44)$$

where $\phi_O : \mathcal{W} - \bigcap_{m=1}^{\mathcal{M}} \mathcal{B}(\boldsymbol{p}_{\pi_m}, r_{\pi_m}) \longrightarrow [0,1)$ denotes the potential that derives a safe motion vector field within the free space $\mathcal{W} - \bigcap_{m=1}^{\mathcal{M}} \mathcal{B}(\boldsymbol{p}_{\pi_m}, r_{\pi_m})$. Notice that $k > 1$ is a design constant, $\gamma(\boldsymbol{x}_O - \boldsymbol{x}_O^d) > 0$ with $\gamma(\boldsymbol{0}) = 0$ represents the attractive potential field to the goal configuration $\boldsymbol{x}_O^d$ and $\beta(\boldsymbol{x}_O) > 0$ with:

$$\lim_{\boldsymbol{x}_O \to \left\{ \substack{\text{Boundary} \\ \text{Obstacles}} \right.} \beta(\boldsymbol{x}_O) = 0 \quad (45)$$

represents the repulsive potential field by the workspace boundary and the obstacle regions. In that respect, it was proven in [70] that $\phi_O(\boldsymbol{x}_O; \boldsymbol{x}_O^d)$ has a global minimum at $\boldsymbol{x}_O^d$ and no other local minima for sufficiently large k. Thus, a feasible path that leads from any initial obstacle-free configuration[6] to the desired configuration might be generated by following the negated gradient of $\phi_O(\boldsymbol{x}_O; \boldsymbol{x}_O^d)$. Consequently, the desired velocity profile at the leader's side is designed as follows:

$$\boldsymbol{v}_{O_L}^d(t) = -K_{NF}\boldsymbol{J}_O^{-1}(\boldsymbol{\eta}_{2,O}) \nabla_{\boldsymbol{x}_O} \phi_O(\boldsymbol{x}_{O_L}(t), \boldsymbol{x}_O^d) \quad (46)$$

where $K_{NF} > 0$ is a positive gain. Therefore, the initial configuration, the leading UVMS may easily calculate the desired trajectory and velocity profile denoted by $\boldsymbol{x}_{O_L}^d(t)$ and $\boldsymbol{v}_{O_L}^d(t)$ respectively, by propagating the model $\dot{\boldsymbol{x}}_{O_L}^d(t) = \boldsymbol{J}_O\big(\boldsymbol{\eta}_{2,O}(t)\big)\boldsymbol{v}_{O_L}^d(t)$.

C. Desired Trajectory Estimation Scheme

It should be noticed that the followers are not aware of either the object's desired trajectory $\boldsymbol{x}_O^d$ or the obstacles' position in the workspace. However, even thought explicit communication among the leader and the followers is not permitted, the followers will estimate the object's desired trajectory profile by $\hat{\boldsymbol{x}}_O^{d_i}(t)\ i \in \mathcal{N}$, via their own state measurements by adopting a prescribed performance estimator. Hence, let us define the error:

$$\boldsymbol{e}_i(t) = \boldsymbol{x}_O(t) - \hat{\boldsymbol{x}}_O^{d_i}(t) \in \mathbb{R}^6,\ i \in \mathcal{N}. \quad (47)$$

The expression of prescribed performance for each element of $\boldsymbol{e}_i(t) = [e_{i1}(t), \ldots, e_{i6}(t)]^\top,\ i \in \mathcal{N}$ is given by the following inequalities:

$$-\rho_{ij}(t) < e_{ij}(t) < \rho_{ij}(t),\ j = 1, \ldots, 6 \text{ and } i \in \mathcal{N} \quad (48)$$

for all $t \geq 0$, where $\rho_{ij}(t),\ j = 1, \ldots, 6$ and $i \in \mathcal{N}$ denote the corresponding performance functions. A candidate exponential performance function could be:

$$\rho_{ij}(t) = (\rho_{ij,0} - \rho_{ij,\infty})e^{-\lambda t} + \rho_{ij,\infty},\ i \in \mathcal{N} \quad (49)$$

where the constant λ dictates the exponential convergence rate, $\rho_{ij,\infty},\ i \in \mathcal{N}$ denotes the ultimate bound and $\rho_{ij,0}$ is chosen to satisfy $\rho_{ij,0} > |e_{ij}(0)|,\ i \in \mathcal{N}$. Hence, following [73], the estimation law is designed as follows:

$$\dot{\hat{x}}_{O_j}^{d_i} = k_{ij} \ln\left(\frac{1 + \frac{e_{ij}(t)}{\rho_{ij}(t)}}{1 - \frac{e_{ij}(t)}{\rho_{ij}(t)}}\right), k_{ij} > 0,\ j = 1, \ldots, 6 \quad (50)$$

for $i \in \mathcal{N}$, from which the followers' estimate $\hat{\boldsymbol{x}}_O^{d_i}(t) = [\hat{\boldsymbol{x}}_{O_1}^{d_i}(t), \ldots, \hat{\boldsymbol{x}}_{O_6}^{d_i}(t)]^\top,\ i \in \mathcal{N}$ is calculated via a simple integration. Moreover, differentiating (50) with respect to time, we acquire the desired acceleration signal:

$$\ddot{\hat{x}}_{O_j}^{d_i} = \frac{2k_{ij}}{1 - \left(\frac{e_{ij}(t)}{\rho_{ij}(t)}\right)^2} \frac{\dot{e}_{ij}(t)\rho_{ij}(t) - e_{ij}(t)\dot{\rho}_{ij}(t)}{\big(\rho_{ij}(t)\big)^2} \quad (51)$$

employing only the velocity $\dot{\boldsymbol{x}}_O(t)$ of the object and not its acceleration which is unmeasurable. Based on the aforementioned estimation of the object's desired trajectory profile $\hat{\boldsymbol{x}}_O^{d_i}(t)$, $\dot{\hat{\boldsymbol{x}}}_O^{d_i}(t)$ and $\ddot{\hat{\boldsymbol{x}}}_O^{d_i}(t),\ i \in \mathcal{N}$, we can easily derive the corresponding desired trajectory profile for the follower's end-effector, as follows:

$$\begin{aligned} \boldsymbol{v}_{O_{F_i}}^{d_i}(t) &= \boldsymbol{J}_O^{-1}(\boldsymbol{\eta}_{2,O})\dot{\hat{\boldsymbol{x}}}_O^{d_i}(t) \\ \dot{\boldsymbol{v}}_{O_{F_i}}^{d_i}(t) &= \boldsymbol{J}_O^{-1}(\boldsymbol{\eta}_{2,O})\ddot{\hat{\boldsymbol{x}}}_O^{d_i} + \dot{\boldsymbol{J}}_O^{-1}(\boldsymbol{\eta}_{2,O})\dot{\hat{\boldsymbol{x}}}_O^{d_i}. \end{aligned} \quad (52)$$

It is worth noting that the aforementioned estimator is more robust against trajectory profiles with non-zero acceleration than previous results presented in [61], [62]. Moreover, the ultimate bounds in (49) can be set arbitrarily small to a value reflecting the resolution of the measurement devices, thus achieving practical convergence of the estimation errors to zero.

Remark 4: The appropriate selection of the performance functions $\rho_{ij}(t)$ imposes transient and steady state performance characteristics on the estimation errors $e_{ij}(t)$, irrespectively of the design parameters $k_{ij}, i \in \mathcal{N},\ j = 1 \ldots, 6$. In particular, for an initial estimation of the object's desired trajectory profile $\hat{\boldsymbol{x}}_O^{d_i}(0)$ and given $\boldsymbol{x}_O(0)$, the performance functions $\rho_{ij}(t),\ i \in \mathcal{N}$ and, $j = 1, \ldots, 6$ are designed such that: i) $-\rho_{ij}(0) < e_{ij}(0) < \rho_{ij}(0)$ and ii) the desired transient and steady state performance specifications are met. On the other hand, extensive simulation studies have revealed that

[6]Except from a set of measure zero [70].

the selection of the control gains $\boldsymbol{K},\ \boldsymbol{\Gamma}_i,\ \boldsymbol{\Gamma}_{d_i},\ i \in \mathcal{K}$ can have positive influence on the closed loop system response in both the control input characteristics (magnitude and slew rate) as well as the evolution of the tracking errors. In particular, decreasing the gain values leads to slow convergence which is improved when adopting higher values, enlarging however the control effort both in magnitude and rate. Thus, an additional fine tuning is needed in real scenarios to retain the required control input signals within the feasible range that can be implemented by the actuators.

Remark 5: In the current literature, the existing approaches for underwater cooperative object transportation, require an accurate common localization system in order to obtain a mutually agreed desired trajectory of the object. This, intuitively means that all agents should have access to an accurate common position of the object in a global frame. On the contrary, our proposed control framework avoids the need of a common localization system since, each follower estimates locally and in a distributed way the desired object trajectory relatively to its own inertial frame, by employing exclusively its own measurements (position, velocity and force/toque). Hence, even if the estimated position of the object differs among the robots, the collaborative task will succeed.

D. Object External Disturbances Estimation Scheme

In view of the object dynamics (12b), it can be concluded that the vector of external disturbances $\boldsymbol{\lambda}_e$ and consequently $\boldsymbol{\lambda}_{e_i}$ in (20) are unknown. Thus, in order to design the impedance control scheme, each UVMS should estimate the aforementioned vector in a distributed way (since explicit communication among UVMSs is not permitted). Therefore, an online estimation method based on the object momentum concept [74] is given in the sequel. In this context, and in view of (20), in order to estimate $\boldsymbol{\lambda}_{e_i}$ locally we define the object equivalent momentum [74] $\boldsymbol{\mu}_i = \boldsymbol{M}_{O_i}\boldsymbol{v}_O$ and the vector $\boldsymbol{\xi}_i(t) \in \mathbb{R}^6$ as:

$$\boldsymbol{\xi}_i(t) = \boldsymbol{K}_\mu \left(\boldsymbol{\mu}_i(t) + \int_{t_0}^{t} \Big(\boldsymbol{C}_{O_i}\boldsymbol{v}_O + \boldsymbol{D}_{O_i}\boldsymbol{v}_O + \boldsymbol{g}_{O_i} - \boldsymbol{\xi}_i(d\tau) \Big) d\tau \right) \tag{53}$$

where $\boldsymbol{K}_\mu$ is a positive definite gain matrix. The time derivative is given by:

$$\dot{\boldsymbol{\xi}}_i(t) = -\boldsymbol{K}_\mu \boldsymbol{\xi}_i(t) + c_i \boldsymbol{K}_\mu \Big(\sum_{i \in \mathcal{K}} \boldsymbol{J}_{iO}^\top \boldsymbol{\lambda}_i + \boldsymbol{\lambda}_e \Big) \tag{54}$$

which represents a low-pass, whose bandwidth can become arbitrarily large by selecting an appropriate matrix gain $\boldsymbol{K}_\mu$. Therefore, for a sufficiently large $\boldsymbol{K}_\mu$, we obtain:

$$\boldsymbol{\xi}_i(t) \approx c_i \Big(\sum_{i \in \mathcal{K}} \boldsymbol{J}_{iO}^\top \boldsymbol{\lambda}_i + \boldsymbol{\lambda}_e \Big) \tag{55}$$

which intuitively means that $\boldsymbol{\xi}_i(t)$ represents the effect of overall external forces exerted on the object (i.e., external disturbances and the forces exerted by all the UVMSs on the object). Consequently, a reliable estimation of $\boldsymbol{\lambda}_{e_i} = c_i \boldsymbol{\lambda}_e$ can be calculated by:

$$\boldsymbol{\lambda}_{e_i} \approx \boldsymbol{\xi}_i(t) - \boldsymbol{J}_{iO}^\top \boldsymbol{\lambda}_i,\ i \in \mathcal{K}. \tag{56}$$

E. Real World Application

As it is evident, in order to guarantee the overall efficiency of the proposed decentralized control scheme, a number of assumptions have been made. In this subsection, we provide a discussion about how these assumptions can be overcome in real world applications. At first, we assume that the each UVMS is equipped with a Force/Torque (F/T) sensor rigidly attached on its end-effector. Eventhough underwater F/T sensors are not very common, especially when compared to the conventional ones (operating in air) , commercial solutions for underwater F/T sensors do exist e.g [75], [76]. Moreover, several research works where underwater F/T sensors were employed can be found in literature e.g [77], [78].

Next, we assume that each UVMS has the necessary actuation capabilities (vehicle and manipulator) in order to be able to exert arbitrary forces and torques on the object along and about any direction. This is actually not a strict assumption, since a UVMS consisting of a 5DoF vehicle actuated in surge, sway, heave, pitch and yaw and a 4DoF arm with the appropriate kinematic chain (e.g., Girona500 [77], [79]), is in fact able to exert the desired forces and torques.

Next, we consider that each UVMS is equipped with the appropriate sensor suite in order to measure its position and velocity. In order for an underwater vehicle to estimate its full state vector i.e 3D position, orientation, linear and angular velocities and accelerations it needs to fuse data from the following sensors: a) Attitude and Heading Reference System (AHRS) for the measurement of 3D linear accelerations, angular velocities and angles, b) Doppler Velocity Log (DVL) sensor for the measurement of 3D linear body velocities, Ultra Short Baseline (USBL) for 3D position with respect to an absolute (i.e the acoustic transpoder) frame, d) a pressure based depth sensor. Additionally, the sensor suite can be further enhanced with the appropriate perception sensors such as standard or RGB-D cameras, as well as Imaging Sonars for a 3D representation of the environment. The aforementioned sensors are de facto standard in underwater robotics and when fused with the appropriate estimators (e.g Kalman Fiters, Complementary Filters,Adaptive Monte Carlo Localization Filters) can deliver accurately the full state vector of the UVMS as well as the representation of the operating workspace including the position of obstacles within. Regarding the position of the arm, simple encoders attached to the joints are enough to compute the kinematic chain of the arm. Hence, the complete state estimation of a UVMS in real world applications is feasible with standard sensor and data fusion technologies.

Regarding the geometry of workspace, the obstacles, the robots as well as the workspace are all modelled by spheres (i.e., we adopt the spherical world representation [70]). In this respect, we considered that the robots operate in a large workspace with sparse obstacles, hence the employed Navigation Function scheme is able to provide a collision free path. Moreover, we have selected the distance among the grasping points on the given object to be at least $2\bar{r}$ in order to avoid inter robot collision. The aforementioned considerations do not affect the theoretical foundation of this work; they are employed for the sake of simplicity and improving the readability

of the paper. However, the proposed control strategy could be extended to more general and complex geometries with more sophisticated models constituting the future research direction.

IV. Simulation Results

The theoretical findings of this work are verified in a simulation environment built in MATLAB® with sampling time $0.1\ sec$, which is a common real time operation cycle for an underwater robotic system. The UVMS model considered in the simulations is an AUV equipped with a small 4 DoFs manipulator attached at the bow of the vehicle (see Fig.4). The design parameters of both the AUV and the robotic manipulator are given in Tables I-III. The dynamics (5) were derived based on the Newton-Euler approach [80] and its numeric evaluation and the calculation of the interaction force/torque vector $\boldsymbol{\lambda_i},\ i \in \mathcal{K}$ were performed following [37]. Finally, the object of interest was a pipe grid whose design parameters are given in Table-IV.

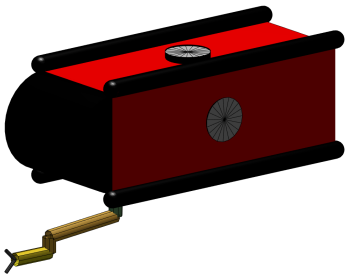

Fig. 4. The UVMS model considered in the simulation studies

TABLE I
VEHICLE PARAMETERS

Parameter	Value	Unit
Degree of freedoms	6	
Length	0.64	m
Height	0.24	m
Width	0.25	m
Mass in air	12	kg

TABLE II
DENAVIT-HARTENBERG PARAMETERS OF THE ROBOTIC ARM

Link	d_i	θ_i	a_i	α_i
1	L_1	q_1	0	$-\frac{\pi}{2}$
2	0	$q_2 - \frac{\pi}{2}$	L_2	0
3	0	$q_3 + \frac{\pi}{2}$	$-L_3$	$\frac{\pi}{2}$
4	L_4	q_4	0	0

The cooperative transportation is performed by 4 UVMSs grasping the object at its corners (see Fig.5). The blue UVMS acts as the leader. Thus, we assume that the desired object's configuration as well as the obstacles' position in the workspace are transferred to the leading UVMS beforehand. The obstacles are modeled as spheres (1 m radius) and are located in the workspace in order to complicate the transportation task of the object. In this respect, a Navigation

TABLE III
PARAMETERS OF THE ROBOTIC ARM

Parameter	Value	Unit
Link 1 Length(L_1)	7.7	cm
Link 2 Length(L_2)	14.7	cm
Link 3 Length(L_3)	2.8	cm
Link 4 Length(L_4)	7.5	cm
Link 1 Mass	0.1	kg
Link 2 Mass	0.2	kg
Link 3 Mass	0.1	kg
Link 4 Mass	0.12	kg
Link Diameter	6	cm

TABLE IV
OBJECT CHARACTERISTICS

Parameter	Value	Unit
Length	1.8	m
Pipe Diameter	5	cm
Mass in Air	1.5	kg

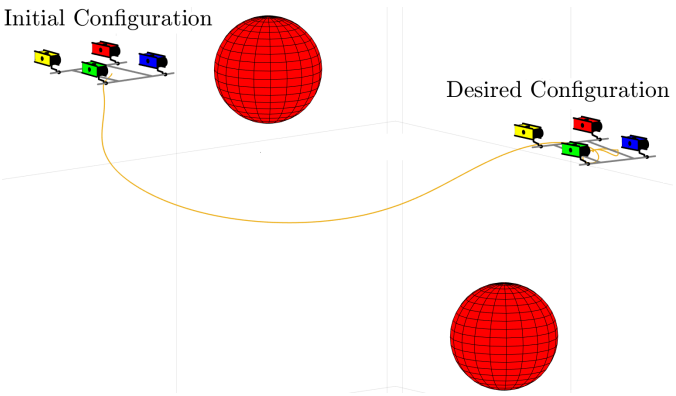

Fig. 5. Four UVMSs transport a rigidly grasped object in a constrained workspace with static obstacles. Only the leading UVMS (indicated with blue color) is aware of the object's desired trajectory. A safe object trajectory in 3D space is indicated by orange color.

Function is constructed following (44) in order to handle the aforementioned constrained workspace. Since only the leading UVMS (blue) is aware of the object's desired configuration, the followers will estimate it via the proposed algorithm (50), by simply observing the motion of the object and without communicating explicitly with the leader. In all subsequent simulations studies, the dynamics of the UVMS were affected by external disturbances in the form of slowly time varying sea currents modeled by the corresponding velocities $v_x^c = 0.3\sin(\frac{\pi}{15}t)\frac{m}{s}$ and $v_y^c = 0.3\cos(\frac{\pi}{15}t)\frac{m}{s}$. Notice that in all of the following simulations we considered parametric uncertainty up to 15% (i.e., the initial estimation of dynamic parameters in differential equation (38) (i.e., $\hat{\boldsymbol{\theta}}_i(0)$) for each UVMS was set with a deviation of 15% form the actual ones employed in the simulation core). The aforementioned uncertainties along with the considered external disturbances constitute the system uncertainty considered during simulation studies. Thus, the adaptive laws (38) and (39) were adopted to provide their estimates with corresponding control gains presented in Table-V.

In the following simulations the control gains and the parameters of the proposed estimator were chosen as shown

in Table-V and Table-VI. Regarding the Navigation Function, the control gains were selected by trial and error procedure. More specifically, gain k (See Table V) has been set large enough in order to avoid local minima. Moreover, the adaptive control gains were also selected by trial and error procedure. In addition, regarding the estimation gains (See Table VI), the design parameters $\rho_{ij,0},\ j = 1,\ldots,6$ can be selected such that the initial estimation retained within the certain bounds. In this direction, the design parameters $\rho_{ij,\infty},\ i \in \mathcal{N}$ and $j = 1,\ldots,6$ of the performance functions $\rho_{ij}(t), i \in \mathcal{N}$ and $j = 1,\ldots,6$ can be set arbitrarily small to a value reflecting the resolution of the measurement device, thus achieving practical convergence of the estimation errors to zero. Additionally, the transient response depends on the convergence rate of the performance functions $\rho_{ij}(t), i \in \mathcal{N}$ and $j = 1,\ldots,6$ that is directly affected by the parameter λ.

TABLE V
CONTROL GAINS OF THE PROPOSED CONTROL SCHEME

Parameter	Value
$\boldsymbol{M}_{d_o},\ i \in \mathcal{K}$	$\boldsymbol{I}_{6\times6}$
$\boldsymbol{D}_{d_o},\ i \in \mathcal{K}$	$\boldsymbol{I}_{6\times6}$
$\boldsymbol{K}_{d_o},\ i \in \mathcal{K}$	$\boldsymbol{I}_{6\times6}$
$\boldsymbol{M}_{d},\ i \in \mathcal{K}$	$\boldsymbol{I}_{6\times6}$
$\boldsymbol{D}_{d},\ i \in \mathcal{K}$	$\boldsymbol{I}_{6\times6}$
$\boldsymbol{K}_{d},\ i \in \mathcal{K}$	$\boldsymbol{I}_{6\times6}$
k (See (44))	12
k_{NF} (See (46))	0.5
$\boldsymbol{\Gamma}_i,\ i \in \mathcal{K}$	$10\boldsymbol{I}_{10\times10}$
$\boldsymbol{\Gamma}_{d_i},\ i \in \mathcal{K}$	$10\boldsymbol{I}_{6\times6}$

TABLE VI
PARAMETERS OF THE PROPOSED ESTIMATOR

Parameter	Value
$k_j^i,\ i \in \mathcal{N},\ j = 1,\ldots,6$	1.2
$\rho_{i1,0},\ i \in \mathcal{N}$	5
$\rho_{i2,0},\ i \in \mathcal{N}$	4
$\rho_{i3,0},\ i \in \mathcal{N}$	4
$\rho_{i4,0},\ i \in \mathcal{N}$	1
$\rho_{i5,0},\ i \in \mathcal{N}$	1
$\rho_{i6,0},\ i \in \mathcal{N}$	1
$\rho_{ij,\infty},\ i \in \mathcal{N},\ j = 1,\ldots,6$	0.03
λ	1

Simulation Study A

The results are illustrated in Figs.6-11. The evolution of the system under the proposed methodology is given in Fig.6. It should be noticed that the UVMSs have transported cooperatively the grasped object from the initial configuration to the desired one without colliding with the obstacles. By observing the object's tracking error (Fig.7) it can be concluded that even under the influence of external disturbances, the errors in all directions converge very close to zero. The estimation errors of the proposed estimation scheme are presented in Fig.8. It can be easily seen that the estimation errors converge smoothly to zero and remain always within the performance envelope defined by the corresponding performance functions as it was expected from the aforementioned theoretical analysis. The evolution of the Navigation Function potential is presented in Fig.9. The value of Navigation Function remains strictly less

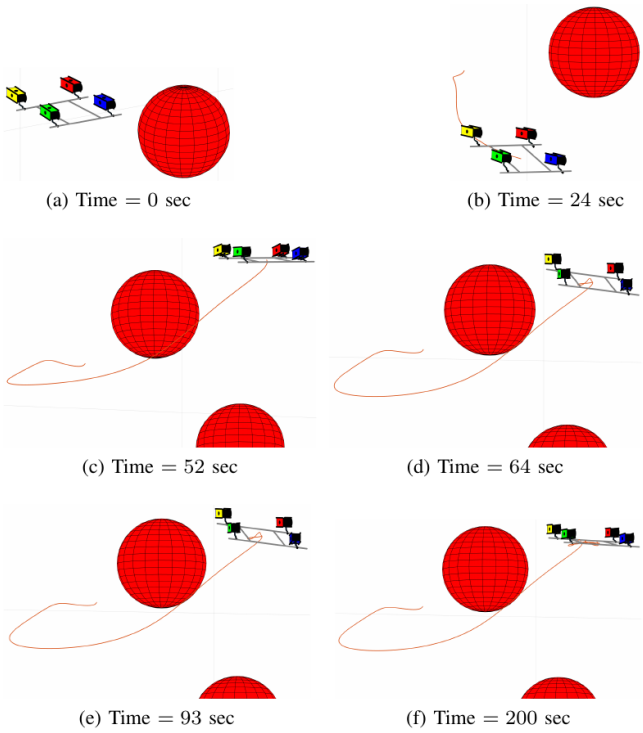

(a) Time = 0 sec (b) Time = 24 sec (c) Time = 52 sec (d) Time = 64 sec (e) Time = 93 sec (f) Time = 200 sec

Fig. 6. Simulation study A: The evolution of the proposed methodology in 6 consecutive time instants.

than 1 during the simulation study which consequently means that collision have been successfully avoided. Moreover, the task space control commands are depicted in Fig-10. As it can be observed, the leading UVMS control inputs at some points are greater with respect to the others robots. This can be explained since the leading UVMS is the only robot aware of the desired configuration of the object, hence it is responsible for navigating the team from a starting to a desired configuration while simultaneously avoid obstacles. Thus, it enforces the whole team to change direction of motion when needed. Finally, Fig. 11 represents the of evolution of the desired and actual force/torque (i.e., $\boldsymbol{\lambda}_i^d$ and $\boldsymbol{\lambda}_i,\ i \in \mathcal{K}$ respectively) exerted by UVMSs on the object.

Simulation study B

We considered exactly the same simulation scenario, but instead a centralized control scheme was implemented to compare its response with the proposed scheme. More specifically, we incorporated the Navigation Function concept within the centralized control scheme presented in [36] (i.e., we modified the proportional term of the control scheme) in order to achieve obstacle avoidance. Observing the error trajectory tracking of Fig.12, it can be concluded that the system under the centralized control scheme reached the desired configuration while avoiding the obstacles within the workspace. However, employing the aforementioned centralized scheme requires 92 variables (i.e., 20 state and velocity variables $\boldsymbol{q}_i$ and $\boldsymbol{\zeta}_i$, $i \in \mathcal{K}$ for each UVMS as well as 12 state and velocity variables for the object) to be exchanged online among the robots. Considering floating point variables, this implemen-

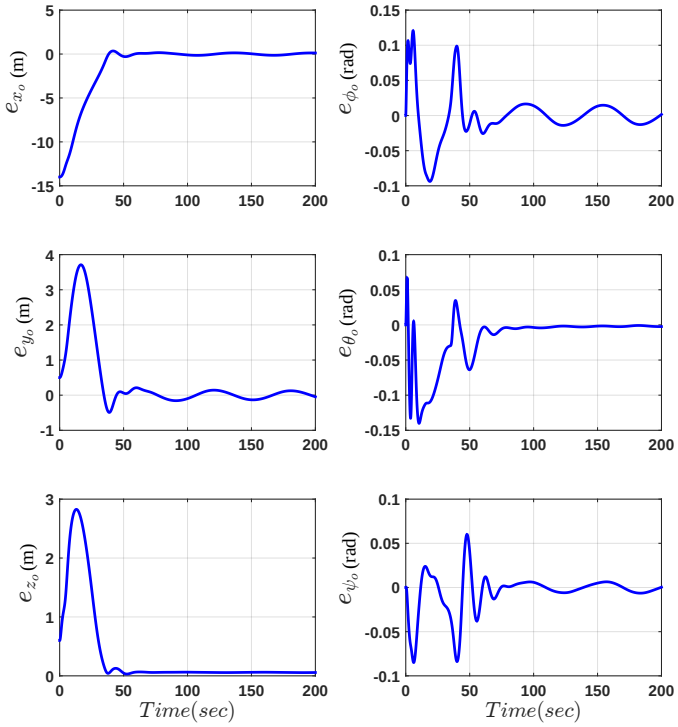

Fig. 7. Simulation study A: The object tracking errors in all directions.

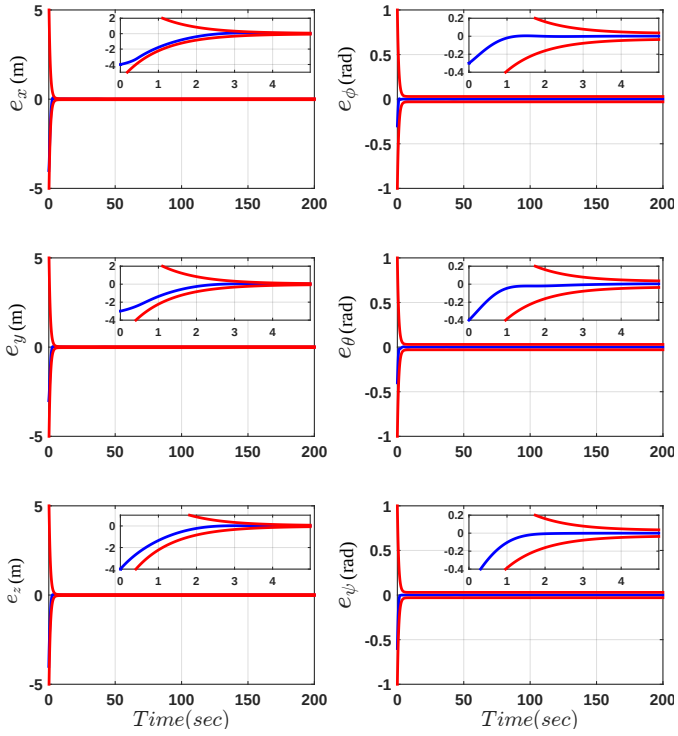

Fig. 8. Simulation study A: The estimation errors along with the performance bounds imposed by the proposed method. The estimation errors and performance bounds are indicated by blue and red color respectively.

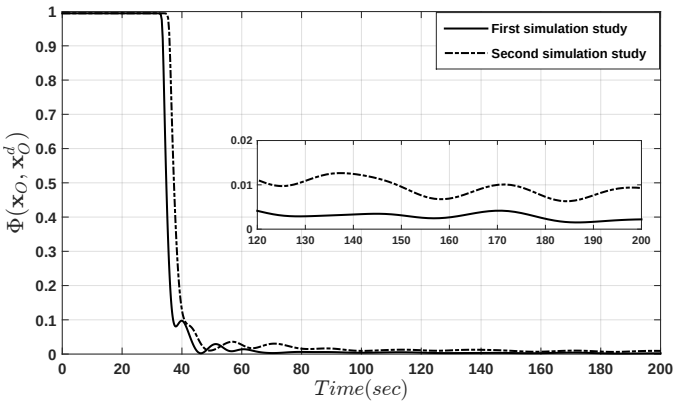

Fig. 9. Simulation studies A-B: The evolution of the Navigation Function potential.

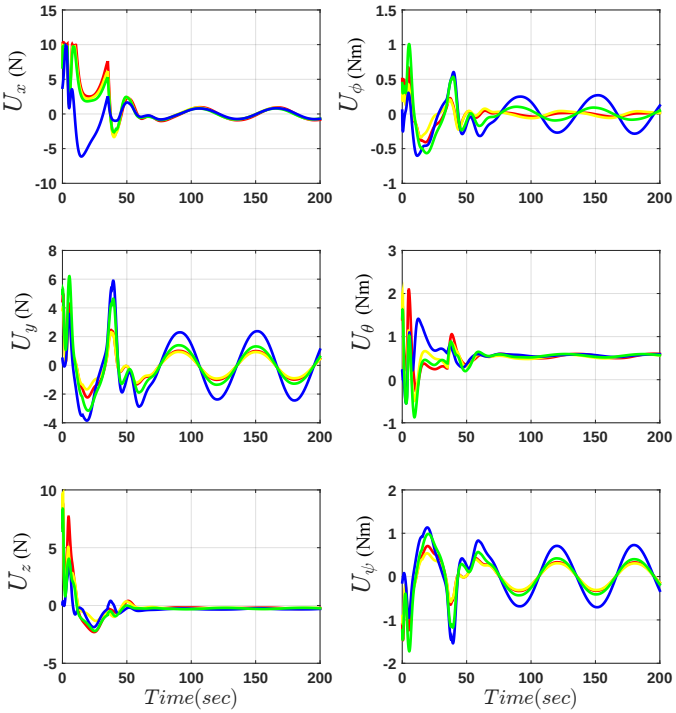

Fig. 10. Simulation study A: The evolution of control inputs. The corresponding control inputs of the leading UVMS is indicated with blue color while the following UVMSs are indicated with red, yellow and green color respectively.

tation requires the transfer of 2944 bytes in every control loop. Therefore, considering a full-duplex communication, in order to achieve a 10 Hz exchanging rate, which is an ordinary rate in underwater robotics, a modem with at least 30 $kbyte/s$ bandwidth capability should be available which is unreasonably demanding based on the current technology in underwater acoustic modems and the small number of cooperating robots. For instance, high speed acoustic modems provided by *Evologics* (e.g., S2C 48/78, S2C 40/80, S2C 42/65) supply data transfer rates up to 31 $kbit/s$. Although, recent advances in underwater acoustic modem technology accomplish continuously higher rate of communication, nevertheless, the number of participating robots remains still small owing to the limited bandwidth. For instance, in the considered

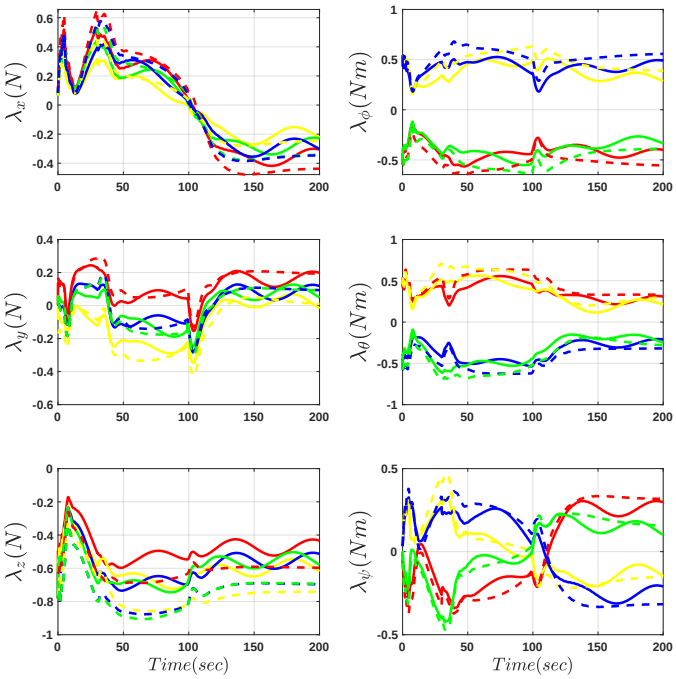

Fig. 11. Simulation study A: The evolution of the desired and actual force/toque exerted by UVMSs on the object. The desired forces/torques ($\boldsymbol{\lambda}_L^d$) leading UVMS is indicated with dashed line in blue while the following UVMSs ($\boldsymbol{\lambda}_i^d,\ i \in \mathcal{N}$) are indicated with dashed lines in red, yellow and green color respectively.

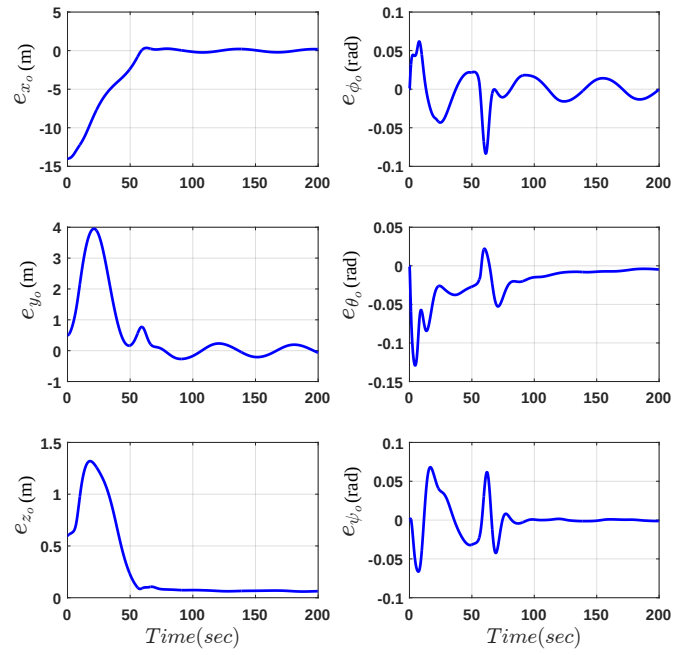

Fig. 12. Simulation study B: The object tracking errors in all directions employing the centralized control scheme presented in [36].

scenario, if the number of cooperating robots increases by one (i.e., 5 cooperative UVMSs), the bandwidth requirements increases respectively up to 35 $kbyte/s$ which would also raise significantly the mission costs. On the contrary, it should be noticed that the proposed control strategy imposes no restriction regarding the underwater communication bandwidth.

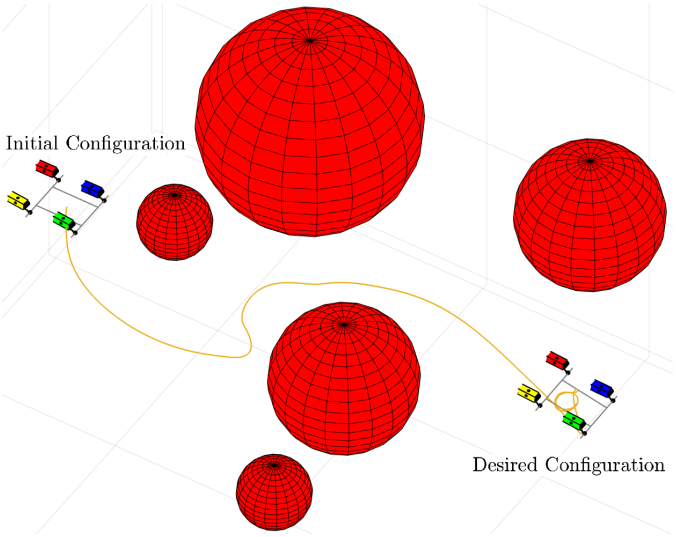

Fig. 13. Simulation study C: The evolution of the object trajectory in 3D space is indicated by orange color.

In addition, if we consider the approach proposed in [55], which to the best our knowledge uses the most restricted information exchange would require 24 variables (i.e., 6 optimal velocity variables calculated by each robot) to be exchanged for the same simulation scenario. considering floating point variables, this implementation requires the transfer of 768 bytes in every control loop in a full-duplex communication in every control loop. Hence, for a 10 Hz exchanging rate, an acoustic modem with at least 10 $kbytes/s$ bandwidth capability should be available. This is certainly more optimal in comparison to the centralized scheme appeared in [36]. However, the requirement bandwidth still remains high, thus, the number of participating robots will inevitably remain low.

Simulation study C

In order to verify the capabilities of the proposed scheme at full extend, a more complex scenario is considered, where more obstacles were involved within the workspace. We kept unaltered the control gains, the estimator parameters and the external disturbances. The object initial and desired configuration are $\boldsymbol{x}_O^{init} = [-8, 0.5, 0.6, 0, 0, 0]^\top$ and $\boldsymbol{x}_O^d = [7, 0, 0, 0, 0, 0]^\top$ respectively. The workspace, initial and desired configuration, as well as the trajectory of the object are illustrated in Fig.13. By observing the object tracking errors (Fig.14), it can be concluded that even in a more complicated case with more obstacles, the team of UVMSs transported successfully the object from the initial to the desired configuration (see Fig.15). The evolution of the task space control signals are presented in Fig 16. Finally, the estimation errors of the proposed estimation scheme are presented in Fig.17. It can be easily seen that the estimation errors converge smoothly to zero and remain always within the performance envelope defined by the corresponding performance functions as it was expected from the aforementioned theoretical analysis. Finally, Fig. 18 represents the of evolution of the desired and actual force/torque (i.e., $\boldsymbol{\lambda}_i^d$ and $\boldsymbol{\lambda}_i,\ i \in \mathcal{K}$ respectively) exerted by UVMSs on the object.

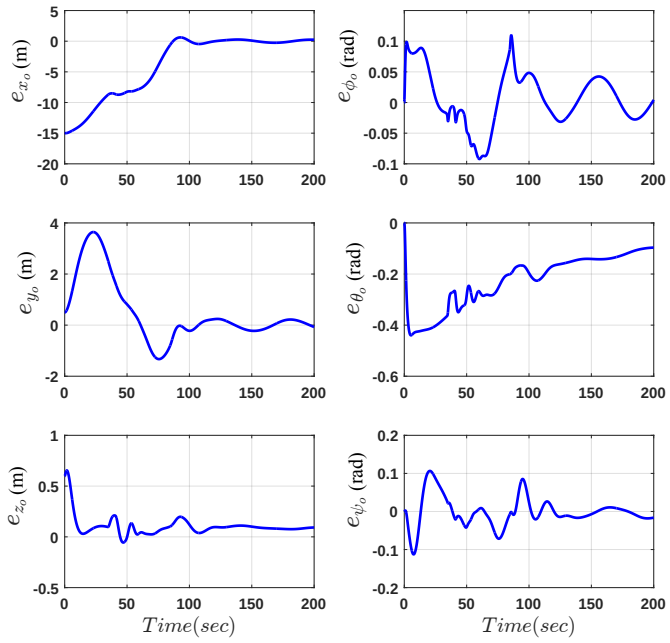

Fig. 14. Simulation study C: The object tracking errors in all directions.

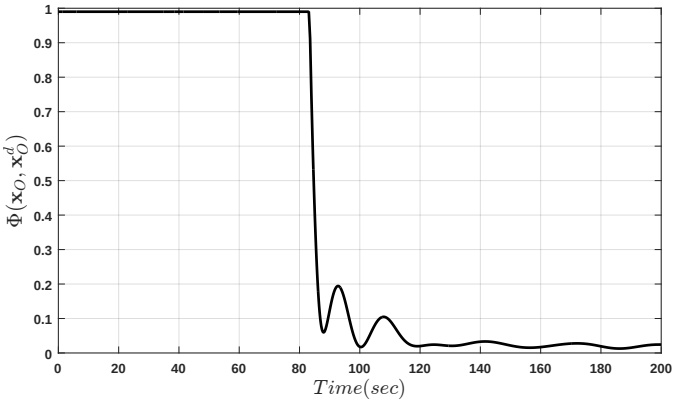

Fig. 15. Simulation study C: The evolution of the Navigation Function.

V. Summary and Future Work

In this work, we presented a cooperative object transportation scheme for Underwater Vehicle Manipulator Systems under implicit communication, avoiding thus completely tedious explicit data transmission. In the proposed scheme, only the leading UVMS is aware of the desired configuration of the object and the obstacles' position in the workspace, and aims at navigating safety the overall formation towards the goal configuration. On the contrary, the followers adopt a prescribed performance estimation technique in order to estimate the object's desired trajectory and implement an impedance control law achieving in this way tracking of the desired trajectory despite the uncertainty and external disturbances in the object and the UVMS dynamics respectively. Each following UVMS employs the proposed estimator based on its own local measurements. Moreover, contrary to the existing work in the related literature, the proposed scheme imposes no restrictions on the underwater communication bandwidth.

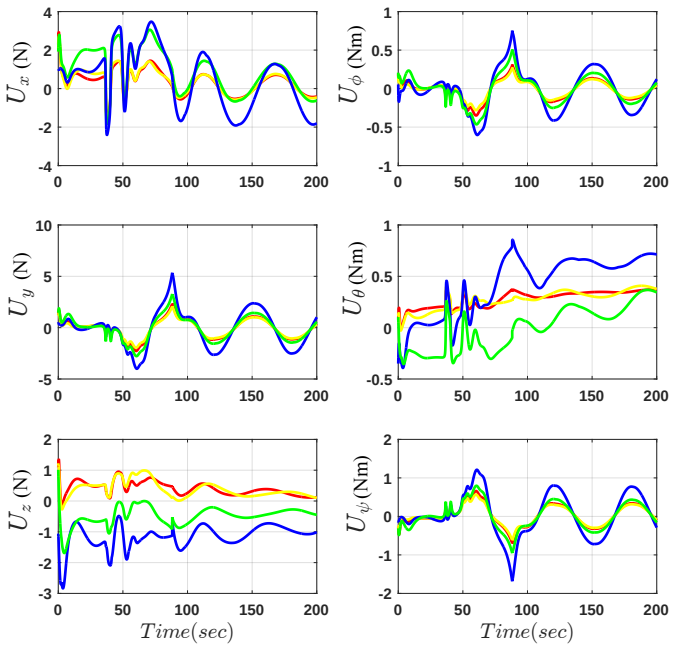

Fig. 16. Simulation study C: Evolution of control inputs. The corresponding control inputs of the leading UVMS is indicated with blue color while the following UVMSs are indicated with red, yellow and green color respectively.

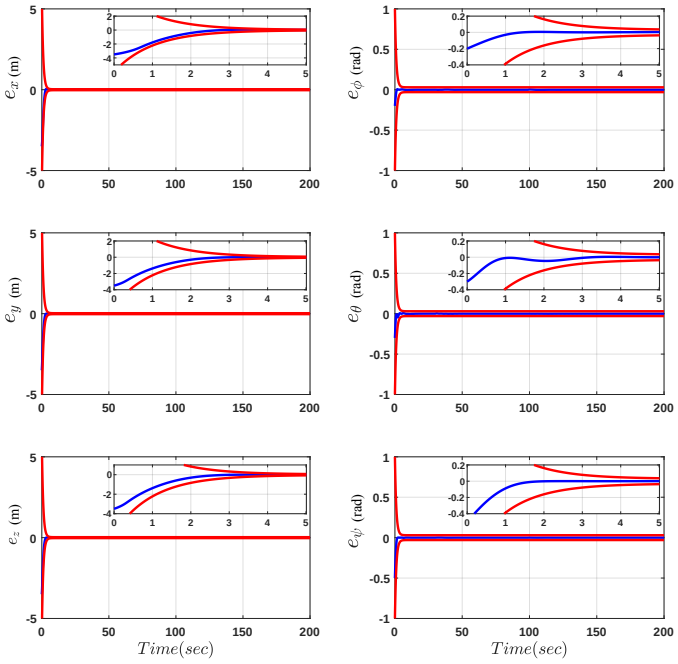

Fig. 17. Simulation study C: The estimation errors along with the performance bounds imposed by the proposed method. The estimation errors and performance bounds are indicated by blue and red color respectively.

Furthermore, the control scheme adopts load sharing among the UVMSs according to their specific payload capabilities. Future research efforts will be devoted towards extending the proposed methodology for multiple UVMSs with underactuated vehicle dynamics.

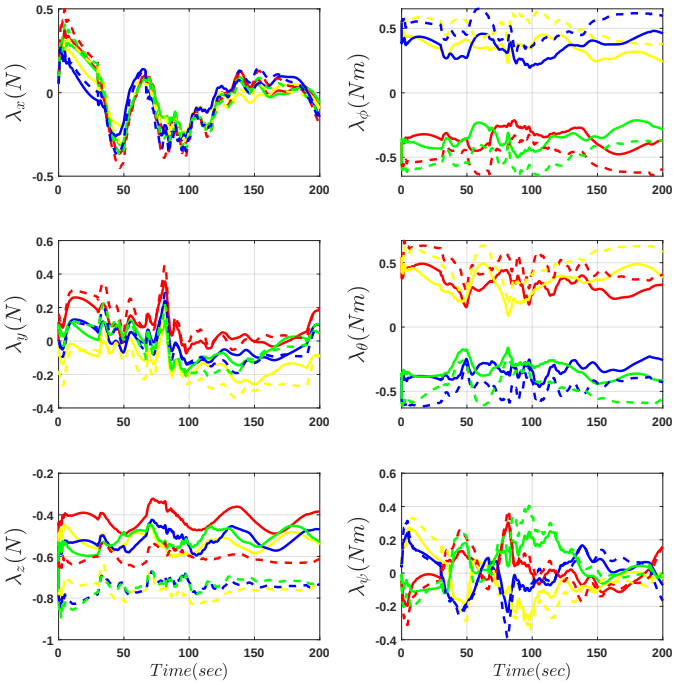

Fig. 18. Simulation study C: The evolution of the desired and actual force/toque exerted by UVMSs on the object. The desired forces/torques ($\boldsymbol{\lambda}_L^d$) leading UVMS is indicated with dashed line in blue while the following UVMSs ($\boldsymbol{\lambda}_i^d,\ i \in \mathcal{N}$) are indicated with dashed lines in red, yellow and green color respectively.

REFERENCES

[1] J. Yuh, "Design and control of autonomous underwater robots: A survey," *Autonomous Robots*, vol. 8, no. 1, pp. 7–24, 2000.

[2] P. Ridao, M. Carreras, D. Ribas, and R. Garcia, "Visual inspection of hydroelectric dams using an autonomous underwater vehicle," *Journal of Field Robotics*, vol. 27, no. 6, pp. 759–778, 2010.

[3] F. Zhang, G. Marani, R. N. Smith, and H. T. Choi, "Future trends in marine robotics [tc spotlight]," *IEEE Robotics Automation Magazine*, vol. 22, pp. 14–122, March 2015.

[4] G. Ferri, A. Munafo, and K. LePage, "An autonomous underwater vehicle data-driven control strategy for target tracking," *IEEE Journal of Oceanic Engineering*, vol. 43, no. 2, pp. 323–343, 2018.

[5] B. Bingham, B. Foley, H. Singh, R. Camilli, K. Delaporta, R. Eustice, A. Mallios, D. Mindell, C. Roman, and D. Sakellariou, "Robotic tools for deep water archaeology: Surveying an ancient shipwreck with an autonomous underwater vehicle," *Journal of Field Robotics*, vol. 27, no. 6, pp. 702–717, 2010.

[6] S. Heshmati-Alamdari, G. C. Karras, P. Marantos, and K. J. Kyriakopoulos, "A robust predictive control approach for underwater robotic vehicles," *IEEE Transactions on Control Systems Technology*, 2019.

[7] X. Xiang, B. Jouvencel, and O. Parodi, "Coordinated formation control of multiple autonomous underwater vehicles for pipeline inspection," *International Journal of Advanced Robotic Systems*, vol. 7, no. 1, pp. 75–84, 2010.

[8] P. Ridao, M. Carreras, D. Ribas, P. Sanz, and G. Oliver, "Intervention auvs: The next challenge," *Annual Reviews in Control*, vol. 40, pp. 227–241, 2015.

[9] H. Farivarnejad and S. Moosavian, "Multiple impedance control for object manipulation by a dual arm underwater vehicle-manipulator system," *Ocean Engineering*, vol. 89, pp. 82–98, 2014.

[10] H. Shim, B.-H. Jun, P.-M. Lee, H. Baek, and J. Lee, "Workspace control system of underwater tele-operated manipulators on an rov," *Ocean Engineering*, vol. 37, no. 11-12, pp. 1036–1047, 2010.

[11] P. Londhe, S. Mohan, B. Patre, and L. Waghmare, "Robust task-space control of an autonomous underwater vehicle-manipulator system by pid-like fuzzy control scheme with disturbance estimator," *Ocean Engineering*, vol. 139, pp. 1–13, 2017.

[12] S. Mohan and J. Kim, "Coordinated motion control in task space of an autonomous underwater vehicle-manipulator system," *Ocean Engineering*, vol. 104, pp. 155–167, 2015.

[13] S. Heshmati-Alamdari, C. P. Bechlioulis, G. C. Karras, A. Nikou, D. V. Dimarogonas, and K. J. Kyriakopoulos, "A robust interaction control approach for underwater vehicle manipulator systems," *Annual Reviews in Control*, vol. 46, pp. 315–325, 2018.

[14] G. Marani, S. Choi, and J. Yuh, "Underwater autonomous manipulation for intervention missions auvs," *Ocean Engineering*, vol. 36, no. 1, pp. 15–23, 2009.

[15] G. Antonelli, *"Underwater Robots"*. Springer Tracts in Advanced Robotics, Springer International Publishing, 2013.

[16] E. Simetti and G. Casalino, "Whole body control of a dual arm underwater vehicle manipulator system," *Annual Reviews in Control*, vol. 40, pp. 191–200, 2015.

[17] D. Lane, D. O'Brien, M. Pickett, J. Davies, G. Robinson, D. Jones, E. Scott, G. Casalino, G. Bartolini, G. Cannata, A. Ferrara, D. Angelleti, M. Coccoli, G. Veruggio, R. Bono, P. Virgili, M. Canals, R. Pallas, E. Gracia, and C. Smith, "Amadeus: Advanced manipulation for deep underwater sampling," *IEEE Robotics and Automation Magazine*, vol. 4, no. 4, pp. 34–45, 1997.

[18] G. Casalino, D. Angeletti, T. Bozzo, and G. Marani, "Dexterous underwater object manipulation via multi-robot cooperating systems," in *Proceedings 2001 icra. ieee international conference on robotics and automation (cat. no. 01ch37164)*, vol. 4, pp. 3220–3225, IEEE, 2001.

[19] V. Rigaud, E. Coste-Manière, M. Aldon, P. Probert, M. Perrier, P. Rives, D. Simon, D. Lane, J. Kiener, A. Casals, J. Amat, P. Dauchez, and M. Chantler, "Union: Underwater intelligent operation and navigation," *IEEE Robotics and Automation Magazine*, vol. 5, no. 1, pp. 25–34, 1998.

[20] P. Sanz, P. Ridao, G. Oliver, G. Casalino, C. Insaurralde, C. Silvestre, C. Melchiorri, and A. Turetta, "Trident: Recent improvements about autonomous underwater intervention missions," *IFAC Proceedings Volumes (IFAC-PapersOnline)*, vol. 3, no. PART 1, pp. 355–360, 2012.

[21] M. Prats, J. Garcia, S. Wirth, D. Ribas, P. Sanz, P. Ridao, N. Gracias, and G. Oliver, "Multipurpose autonomous underwater intervention: A systems integration perspective," *2012 20th Mediterranean Conference on Control and Automation, MED 2012*, pp. 1379–1384, 2012.

[22] J. Fernández, M. Prats, P. Sanz, J. García, R. Marín, M. Robinson, D. Ribas, and P. Ridao, "Grasping for the seabed: Developing a new underwater robot arm for shallow-water intervention," *IEEE Robotics and Automation Magazine*, vol. 20, no. 4, pp. 121–130, 2013.

[23] E. Simetti, G. Casalino, S. Torelli, A. Sperindé, and A. Turetta, "Floating underwater manipulation: Developed control methodology and experimental validation within the trident project," *Journal of Field Robotics*, vol. 31, no. 3, pp. 364–385, 2014.

[24] M. Prats, D. Ribas, N. Palomeras, J. García, V. Nannen, S. Wirth, J. Fernández, J. Beltrán, R. Campos, P. Ridao, P. Sanz, G. Oliver, M. Carreras, N. Gracias, R. Marín, and A. Ortiz, "Reconfigurable auv for intervention missions: A case study on underwater object recovery," *Intelligent Service Robotics*, vol. 5, no. 1, pp. 19–31, 2012.

[25] D. Ribas, P. Ridao, A. Turetta, C. Melchiorri, G. Palli, J. Fernandez, and P. Sanz, "I-auv mechatronics integration for the trident fp7 project," *IEEE/ASME Transactions on Mechatronics*, vol. 20, no. 5, pp. 2583–2592, 2015.

[26] E. Simetti, F. Wanderlingh, S. Torelli, M. Bibuli, A. Odetti, G. Bruzzone, D. L. Rizzini, J. Aleotti, G. Palli, L. Moriello, *et al.*, "Autonomous underwater intervention: Experimental results of the maris project," *IEEE Journal of Oceanic Engineering*, vol. 43, no. 3, pp. 620–639, 2017.

[27] D. Lane, F. Maurelli, P. Kormushev, M. Carreras, M. Fox, and K. Kyriakopoulos, "Persistent autonomy: The challenges of the pandora project," *IFAC Proceedings Volumes (IFAC-PapersOnline)*, vol. 9, no. PART 1, pp. 268–273, 2012.

[28] A. Carrera, N. Palomeras, D. Ribas, P. Kormushev, and M. Carreras, "An intervention-auv learns how to perform an underwater valve turning," *OCEANS 2014 - TAIPEI*, 2014.

[29] A. Carrera, N. Palomeras, N. Hurtos, P. Kormushev, and M. Carreras, "Learning multiple strategies to perform a valve turning with underwater currents using an i-auv," *MTS/IEEE OCEANS 2015 - Genova: Discovering Sustainable Ocean Energy for a New World*, 2015.

[30] A. Birk, T. Doernbach, C. Mueller, T. Łuczynski, A. G. Chavez, D. Koehntopp, A. Kupcsik, S. Calinon, A. K. Tanwani, G. Antonelli, *et al.*, "Dexterous underwater manipulation from onshore locations: Streamlining efficiencies for remotely operated underwater vehicles," *IEEE Robotics & Automation Magazine*, vol. 25, no. 4, pp. 24–33, 2018.

[31] J. Gancet, D. Urbina, P. Letier, M. Ilzokvitz, P. Weiss, F. Gauch, G. Antonelli, G. Indiveri, G. Casalino, A. Birk, M. Pfingsthorn, S. Calinon,

A. Tanwani, A. Turetta, C. Walen, and L. Guilpain, "Dexrov: Dexterous undersea inspection and maintenance in presence of communication latencies," *IFAC-PapersOnLine*, vol. 28, no. 2, pp. 218–223, 2015.

[32] E. Simetti, G. Casalino, F. Wanderlingh, and M. Aicardi, "Task priority control of underwater intervention systems: Theory and applications," *Ocean Engineering*, vol. 164, pp. 40–54, 2018.

[33] P. Di Lillo, E. Simetti, F. Wanderlingh, G. Casalino, and G. Antonelli, "Underwater intervention with remote supervision via satellite communication: Developed control architecture and experimental results within the dexrov project," *IEEE Transactions on Control Systems Technology*, 2020.

[34] "Seaclear website, 2020." https://seaclear-project.eu/. [Online; accessed 01-March-2020],(2020).

[35] T. Padir and A. Koivo, "Modeling of two underwater vehicles with manipulators on-board," *In Proceedings of the IEEE International Conference on Systems, Man and Cybernetics*, vol. 2, pp. 1359–1364, 2003.

[36] Y. Sun and C. Cheah, "Coordinated control of multiple cooperative underwater vehicle-manipulator systems holding a common load," *In Proceedings of the IEEE Techno-Ocean '04: Bridges across the Oceans*, vol. 3, pp. 1542–1547, 2004.

[37] N. McClamroch, "Singular systems of differential equations as dynamic models for constrained robot systems.," *In Proceedings of the IEEE International Conference on Robotics and Automation.*, pp. 21–28, 1986.

[38] T. Padir, "Kinematic redundancy resolution for two cooperating underwater vehicles with on-board manipulators," *In Proceedings of the IEEE International Conference on Systems, Man and Cybernetics*, pp. 3137–3142, 2005.

[39] T. Padir and J. Nolff, "Manipulability and maneuverability ellipsoids for two cooperating underwater vehicles with on-board manipulators," *In Proceedings of the IEEE International Conference on Systems, Man and Cybernetics*, pp. 3656–3661, 2007.

[40] R. Cui, S. Ge, B. Voon Ee How, and Y. Sang Choo, "Leader-follower formation control of underactuated autonomous underwater vehicles," *Ocean Engineering*, vol. 37, no. 17-18, pp. 1491–1502, 2010.

[41] G. Pereira, B. Pimentel, L. Chaimowicz, and M. Campos, "Coordination of multiple mobile robots in an object carrying task using implicit communication," *In Proceedings of the IEEE International Conference on Robotics and Automation*, pp. 281–286, 2002.

[42] D. J. Stilwell and B. E. Bishop, "Framework for decentralized control of autonomous vehicles," *In Proceedings of the IEEE International Conference on Robotics and Automation*, vol. 3, pp. 2358–2363, 2000.

[43] M. Uchiyama and P. Dauchez, "Symmetric hybrid position/force control scheme for the coordination of two robots.," *In Proceedings of the IEEE International Conference on Robotics and Automation.*, pp. 350–356, 1988.

[44] O. Khatib, "Object manipulation in a multi-effector robot system," *in proceeding of the 4th International Symposium on Robotic Research*, vol. 4, pp. 137–144, 1988.

[45] H. Tanner, S. Loizou, and K. Kyriakopoulos, "Nonholonomic navigation and control of cooperating mobile manipulators," *IEEE Transactions on Robotics and Automation*, vol. 19, no. 1, pp. 53–64, 2003.

[46] S. Schneider and J. Cannon, R.H., "Object impedance control for cooperative manipulation: Theory and experimental results," *IEEE Transactions on Robotics and Automation*, vol. 8, no. 3, pp. 383–394, 1992.

[47] A. Nikou, C. Verginis, S. Heshmati-Alamdari, and D. Dimarogonas, "A nonlinear model predictive control scheme for cooperative manipulation with singularity and collision avoidance," pp. 707–712, 2017.

[48] J. Luh and Y. Zheng, "Constrained relations between two coordinated industrial robots for motion control.," *International Journal of Robotics Research*, vol. 6, no. 3, pp. 60–70, 1987.

[49] T. Sugar and V. Kumar, "Decentralized control of cooperating mobile manipulators," *Proceedings - IEEE International Conference on Robotics and Automation*, vol. 4, pp. 2916–2921, 1998.

[50] O. Khatib, K. Yokoi, K. Chang, D. Ruspini, R. Holmberg, and A. Casal, "Vehicle/arm coordination and multiple mobile manipulator decentralized cooperation," *IEEE International Conference on Intelligent Robots and Systems*, vol. 2, pp. 546–553, 1996.

[51] W. C. Dickson, R. H. Cannon Jr., and S. M. Rock, "Decentralized object impedance controller for object/robot-team systems: Theory and experiments," *In Proceedings of the IEEE International Conference on Robotics and Automation*, vol. 4, pp. 3589–3596, 1997.

[52] Y.-H. Liu, S. Arimoto, and T. Ogasawara, "Decentralized cooperation control: non-communication object handling," *In Proceedings of the IEEE International Conference on Robotics and Automation*, vol. 3, pp. 2414–2419, 1996.

[53] R. Conti, E. Meli, A. Ridolfi, and B. Allotta, "An innovative decentralized strategy for i-auvs cooperative manipulation tasks," *Robotics and Autonomous Systems*, vol. 72, pp. 261–276, 2015.

[54] R. Furferi, R. Conti, E. Meli, and A. Ridolfi, "Optimization of potential field method parameters through networks for swarm cooperative manipulation tasks," *International Journal of Advanced Robotic Systems*, vol. 13, no. 5, pp. 1–13, 2016.

[55] E. Simetti and G. Casalino, "Manipulation and transportation with cooperative underwater vehicle manipulator systems," *IEEE Journal of Oceanic Engineering*, 2016.

[56] N. Manerikar, G. Casalino, E. Simetti, S. Torelli, and A. Sperindé, "On autonomous cooperative underwater floating manipulation systems," *In Proceedings of the IEEE International Conference on Robotics and Automation*, vol. 2015-June, 2015.

[57] N. Manerikar, G. Casalino, E. Simetti, S. Torelli, and A. Sperinde, "On cooperation between autonomous underwater floating manipulation systems," *2015 IEEE Underwater Technology, UT 2015*, 2015.

[58] E. Simetti and G. Casalino, "A novel practical technique to integrate inequality control objectives and task transitions in priority based control," *Journal of Intelligent and Robotic Systems: Theory and Applications*, vol. 84, no. 1-4, pp. 877–902, 2016.

[59] S. Heshmati-Alamdari, C. P. Bechlioulis, G. C. Karras, and K. J. Kyriakopoulos, "Decentralized impedance control for cooperative manipulation of multiple underwater vehicle manipulator systems under lean communication," in *Autonomous Underwater Vehicles (AUV), 2018 IEEE/OES*, pp. –, IEEE, 2018.

[60] C. Bechlioulis and G. Rovithakis, "Prescribed performance adaptive control for multi-input multi-output affine in the control nonlinear systems," *IEEE Transactions on Automatic Control*, vol. 55, no. 5, pp. 1220–1226, 2010.

[61] K. Kosuge, T. Oosumi, and H. Seki, "Decentralized control of multiple manipulators handling an object in coordination based on impedance control of each arm," *IEEE International Conference on Intelligent Robots and Systems*, vol. 1, pp. 17–22, 1997.

[62] K. Kosuge, T. Oosumi, and K. Chiba, "Load sharing of decentralized-controlled multiple mobile robots handling a single object," *In Proceedings of the IEEE International Conference on Robotics and Automation*, vol. 4, 1997.

[63] L. Sciavicco and B. Siciliano, *Modelling and control of robot manipulators*. Springer Science & Business Media, 2012.

[64] B. Siciliano, L. Sciavicco, and L. Villani, *Robotics : modelling, planning and control*. Advanced Textbooks in Control and Signal Processing, Springer, 2009. 013-81159.

[65] S. Soylu, B. Buckham, and R. Podhorodeski, "Redundancy resolution for underwater mobile manipulators," *Ocean Engineering*, vol. 37, no. 2-3, pp. 325–343, 2010.

[66] M. Jallouli, M. Boukattaya, and T. Damak, "Dynamic redundancy resolution for mobile manipulators with joints velocity limits avoidance," in *2008 5th International Multi-Conference on Systems, Signals and Devices*, pp. 1–6, July 2008.

[67] G. D. White, R. M. Bhatt, C. P. Tang, and V. N. Krovi, "Experimental evaluation of dynamic redundancy resolution in a nonholonomic wheeled mobile manipulator," *IEEE/ASME Transactions on Mechatronics*, vol. 14, pp. 349–357, June 2009.

[68] J.-J. E. Slotine and W. Li, "Adaptive strategies in constrained manipulation.," *In Proceedings of the IEEE International Conference on Robotics and Automation.*, pp. 595–601, 1987.

[69] E. Tatlicioglu, D. Braganza, T. Burg, and D. Dawson, "Adaptive control of redundant robot manipulators with sub-task objectives," *Robotica*, vol. 27, no. 6, pp. 873–881, 2009.

[70] D. Koditschek and E. Rimon, "Robot navigation functions on manifolds with boundary," *Advances in Applied Mathematics*, vol. 11, no. 4, pp. 412–442, 1990.

[71] F. Caccavale, C. Natale, B. Siciliano, and L. Villani, "Resolved-acceleration control of robot manipulators: A critical review with experiments," *Robotica*, vol. 16, no. 5, pp. 565–573, 1998.

[72] R. J. Anderson and M. W. Spong, "Hybrid impedance control of robotic manipulators," *IEEE Journal on Robotics and Automation*, vol. 4, no. 5, pp. 549–556, 1988.

[73] C. P. Bechlioulis and K. J. Kyriakopoulos, "Collaborative multi-robot transportation in obstacle-cluttered environments via implicit communication," *Frontiers in Robotics and AI*, vol. 5, p. 90, 2018.

[74] A. De Luca and R. Mattone, "Sensorless robot collision detection and hybrid force/motion control," in *Robotics and Automation, 2005. ICRA 2005. Proceedings of the 2005 IEEE International Conference on*, pp. 999–1004, IEEE, 2005.

[75] "Udw3 underwater force/torque sensor." http://www.a-tech.ca/Product/Series/866/UDW3_Underwater_Sensor?tab=1. [Online; accessed 14-March-2020],(2020).

[76] "F/t sensor: Delta ip68." https://www.ati-ia.com/products/ft/ft_models.aspx?id=Delta+IP68. [Online; accessed 14-March-2020],(2020).

[77] N. Palomeras, A. Carrera, N. Hurtós, G. C. Karras, C. P. Bechlioulis, M. Cashmore, D. Magazzeni, D. Long, M. Fox, K. J. Kyriakopoulos, *et al.*, "Toward persistent autonomous intervention in a subsea panel," *Autonomous Robots*, vol. 40, no. 7, pp. 1279–1306, 2016.

[78] A. Birk, T. Doernbach, C. Mueller, T. Łuczynski, A. Gomez Chavez, D. Koehntopp, A. Kupcsik, S. Calinon, A. K. Tanwani, G. Antonelli, P. Di Lillo, E. Simetti, G. Casalino, G. Indiveri, L. Ostuni, A. Turetta, A. Caffaz, P. Weiss, T. Gobert, B. Chemisky, J. Gancet, T. Siedel, S. Govindaraj, X. Martinez, and P. Letier, "Dexterous underwater manipulation from onshore locations: Streamlining efficiencies for remotely operated underwater vehicles," *IEEE Robotics Automation Magazine*, vol. 25, pp. 24–33, Dec 2018.

[79] D. Ribas, N. Palomeras, P. Ridao, M. Carreras, and A. Mallios, "Girona 500 auv: From survey to intervention," *IEEE/ASME Transactions on Mechatronics*, vol. 17, pp. 46–53, Feb 2012.

[80] I. Schjølberg and T. I. Fossen, "Modelling and control of underwater vehicle-manipulator systems," *in Proc. rd Conf. on Marine Craft maneuvering and control*, pp. 45–57, 1994.